2018

Secondary Functions And Novel Inhibitors Of Aminoacyl-Trna Synthetases

Patrick Wiencek
University of Vermont

SECONDARY FUNCTIONS AND NOVEL INHIBITORS OF AMINOACYL-TRNA SYNTHETASES

A Thesis Presented

by

Patrick Wiencek

to

The Faculty of the Graduate College

of

The University of Vermont

In Partial Fulfillment of the Requirements
for the Degree of Master of Science
Specializing in Biochemistry

October, 2018

Defense Date: June 29, 2018
Thesis Examination Committee:

Christopher S. Francklyn, Ph.D., Advisor
Karen M. Lounsbury, Ph.D., Chairperson
Robert J. Hondal, Ph.D.
Jay Silveira, Ph.D.
Cynthia J. Forehand, Ph.D., Dean of the Graduate College

ABSTRACT

The aminoacyl-tRNA synthetases are a family of enzymes involved in the process of translation, more specifically, ligating amino acids to their cognate tRNA molecules. Recent evidence suggests that aminoacyl-tRNA synthetases are capable of aminoacylating proteins, some of which are involved in the autophagy pathway. Here, we test the conditions under which *E. coli* and human threonyl-tRNA synthetases, as well as hisidyl-tRNA synthetase aminoacylate themselves. These reactions are ATP dependent, stimulated by Mg^{2+}, and are inhibited by increasing cognate tRNA concentrations. These data represent the foundation for future aminoacylation experiments, specifically delving into the relationship between the autophagy pathway and the aminoacylation of proteins.

Additionally, we provide evidence of the inhibitory abilities of the anti-bacterial β-lactone obafluorin on both *E. coli* and human threonyl-tRNA synthetases. Further, we also show that the benzoate obafluorin analog EHTS-1 significantly inhibits *E. coli* threonyl-tRNA synthetase but not the human enzyme. These data could be useful in determining the potential for obafluorin and EHTS-1 as anti-bacterial and possibly anti-angiogenic drugs.

ACKNOWLEDGEMENTS

Dr. Francklyn, thank you for the support, direction, and confidence that you've invested in me over the past two years. Your dedication to helping me complete this program and the projects that we've worked on has helped me irreplaceably in getting to where I am today. It is nothing short of inspiring to have been able to work for and with a PI that is so curious and knowledgeable about their subject matter, dedicated to their students, and passionate about their work. I couldn't have picked a better lab for my Master's program.

My lab mates, more specifically Jamie, Pat Mullen and Terry, thank you so much for all the advice, help, and support (both lab and non-lab related) that you've given me. Jamie, I never would have been able to do any sort of protein purification or kinetics without you, and you taught me to always make sure I heard what you said before I react, all things that I wouldn't be here without. Pat Mullen, thank you for all the jam sessions, conversations, and for letting me help you with your VARS project. Working with you was a phenomenal opportunity, and I'd like to think I played a role in your meteoric return to Soundcloud glory. Terry, thank you for all of the tireless work you put in to make everything run smoothly, and thank you for being a constant reminder that there is someone who can and does work much harder than me. You all have been great friends and lab mates, and I truly enjoyed and appreciated all the time we spend working together.

Dr. Lounsbury, Dr. Silveira, Dr. Hondal, and Dr. Everse, thank you for all of the help, advice, and support that you've given me on this thesis, in classes, in lab meeting, and just as scientists. I appreciate and am inspired by all the effort you've put into me and ensuring the success of your students. Without you I surely wouldn't have made it into the biochemistry AMP program.

TABLE OF CONTENTS

LIST OF TABLES

LIST OF FIGURES

LIST OF ABBREVIATIONS

ARS – Aminoacyl-tRNA Synthetases
Autorad - Autoradiography
Cys - Cysteine
FBS – Fetal Bovine Serum
HARS – Histidyl aminoacyl-tRNA synthetase
IPTG – Isopropyl β-D-1-thiogalactopyranoside
KARS – Lysyl aminoacyl-tRNA synthetase
LC3 – 1A/1B Light Chain 3B
Leu - Leucine
MetRS – Bacterial Methionyl-tRNA Synthetase
mTORC1 – mammalian target of rapamycin complex 1
PAS – Preautophagosome
PE - Phosphatidyl Ethanolamine
PI3P - Phosphatidylinositol 3-phosphate
SDS PAGE – SDS PolyAcrylamide Gel Electrophoresis
TARS – Threonyl-tRNA Synthetase
Thr – Threonine
Val – Valine

CHAPTER 1: INTRODUCTION

1.1. The Primary Function of Aminoacyl-tRNA Synthetases

1.1.1. Aminoacyl-tRNA Synthetases Are Instrumental in Translation

Translation, the process of converting the language of nucleic acids into a sequence of amino acids, is crucial for all forms of life and is dependent on amino acids being charged onto their cognate tRNA molecules with fidelity to the genetic code. Aminoacyl tRNA synthetases (ARS) are a class of enzymes whose canonical function is to ligate an amino acid onto the 3' end of the corresponding tRNA molecule, assisting in the translation of the universal genetic code. Due to this pivotal role in the translational process, ARS are conserved across all the kingdoms of life[1].

ARSs are divided into two classes based on several criteria. Class I ARSs are mostly monomeric, bind tRNA in the minor groove of their acceptor stems, and attach the amino acid to the 2' hydroxyl group of tRNA while class II ARSs are mostly dimeric or multimeric, bind tRNA in the major groove of their acceptor stems, and attach the amino acid to the 3' hydroxyl group of tRNA[2–5]. Class I synthetases tend to interact with the less polar and larger amino acids while class II synthetases tend to interact with the more polar and smaller amino acids. Active site architecture also plays a role in synthetase classification; class I synthetases contain a Rossmann fold, which is shared with kinases and dehydrogenases, while class II synthetases have a six-stranded antiparallel β-sheet fold surrounded by α-helices in their active sites[2,4]. Research indicates that the separate classes of ARSs may have originated from opposite strands of the same ancestral gene[6,7].

ARSs add amino acids to their cognate tRNA molecules in a two-step reaction[3], shown below:

I) Amino acid + ATP ⇌ Aminoacyl-AMP + PP_i

II) Aminoacyl-AMP + tRNA ⇌ Aminoacyl-tRNA + AMP

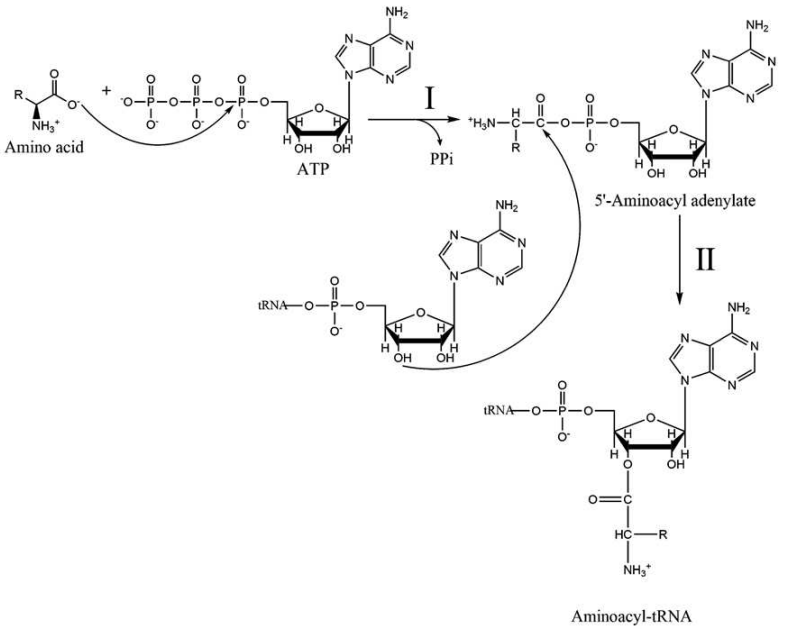

Figure 1. The Mechanism of the Aminoacylation Reaction[8]. Adapted from Li et al., 2015.

In the first step, the ARS 'activates' the amino acid as the carbonyl group of the amino acid attacks the α-phosphate group of ATP, producing an aminoacyl-adenylate intermediate and a pyrophosphate (PP_i) molecule (Figure 1). The aminoacyl-adenylate intermediate remains non-covalently bound to the synthetase following the first of the two-step reaction. In the second step, the 2' or 3' hydroxyl group of the adenine of the tRNA molecule's CCA acceptor stem will attack the carbonyl carbon of the amino acid in the aminoacyl-adenylate, releasing the aminoacylated tRNA molecule and an AMP molecule (Figure 1). This reaction is crucial for protein translation, because the formation of a peptide bond between

two free amino acids is thermodynamically unfavorable[3]. When coupled with the hydrolysis of ATP to AMP and PP_i, the $\Delta G^{o'}$ for the formation of aminoacyl-tRNA is close to zero, which then allows the hydrolysis of PP_i to $2P_i$ to drive the reaction forward. Because of this hydrolysis, the equivalent of 2 ATP molecules are consumed in the aminoacylation reaction.

Because of their pivotal role in carrying out the genetic code, aminoacylation reactions must occur with a high rate of fidelity to minimize translational errors. Mischarged amino acids and translational errors have been associated with cell death in microbes and disease in humans[9–11]. ARSs can distinguish amino acids with discrimination factors from 10,000-100,000, making errors in only 1 of 40,000 aminoacylation reactions[12,13]. This is facilitated by the 'double-sieve model' editing process, first postulated by Fersht in 1979, by which larger amino acids are first discriminated by the active site of the enzyme before smaller near-cognate amino acids are filtered out by a secondary editing domain[14,15]. Fersht published in 1976 that valyl-tRNA synthetase (VARS) was capable of forming a threonyl adenylate but would not catalyze the formation of threonyl-$tRNA^{Val}$ [16]. The editing process for the smaller near-cognate amino acids will either be pre-transfer, where the near-cognate aminoacyl adenylate is hydrolyzed, or post-transfer, where the bond between the mischarged tRNA and the near-cognate amino acid is hydrolyzed. Enzyme kinetics and the presence of tRNA have been determined as deciding factors in whether pre- or post-transfer editing will occur, with pre-transfer editing occurring only when the rate of transfer is significantly slow[17].

Despite performing their canonical function of aminoacylating tRNA, non-canonical functions have been discovered for many of the ARSs. These non-canonical functions include regulation of both glucose and amino acid metabolism, organ development, angiogenesis, inflammatory responses, stress responses, apoptosis, and immune responses[18]. These secondary functions can also be carried out by alternatively spliced or proteolytically cleaved fragments of the full length protein[19].

1.1.2 Aminoacyl-tRNA Synthetases in Disease

Given the essential role of ARS in protein translation, it is unsurprising that disrupting ARS function often results in abnormal cellular homeostasis and disease. ARSs must not only charge tRNA with amino acids, they must do so with high fidelity, and problems with either ARS function or editing could manifest with a phenotype. High levels of mischarged amino acids have been shown to cause toxic effects in both prokaryotic and eukaryotic cells[9–11,20]. A study of the effects of increased amino acid levels on an editing-defective LeuRS mutant *E. coli* strain demonstrated that increased mischarged-tRNA levels inhibited the growth of affected cells[11]. Several different cytoplasmic ARS have been linked to tumor progression, due in part to their crucial function in protein synthesis, supporting cancer proliferation and suppressing apoptotic signals[21,22].

Both dominant and recessive ARS mutations have been linked to a variety of human diseases, which often involve neurological dysfunction[9,23]. Dominant ARS mutations are associated with the peripheral neuropathy known as Charcot-Marie-Tooth disease (CMT), while recessive mutations often cause profound neurodevelopmental

disease characterized by microcephaly and epilepsy[9,23]. CMT is an inherited disease of the peripheral nervous system that causes degeneration of distal motor and sensory neurons in a length dependent manner[24]. This eventually leads to muscle weakness and atrophy in the legs and arms[9,24]. In 2003, Antonellis et al. discovered the first ARS mutations associated with CMT, identifying four glycyl-tRNA variants[25]. Since then, mutations in lysyl-tRNA synthetase, alanyl-tRNA synthetase, tyrosyl-tRNA synthetase, histidyl-tRNA synthetase (HARS) and tryptophanyl-tRNA synthetase have been linked to CMT[9,26]. Although it may seem likely that a unifying pathogenic mechanism links ARS to CMT, some reports suggest that reduced aminoacylation and defective global protein synthesis may not be the underlying cause[26,27].

In addition to dominant ARS mutations linked to CMT, a number of recessive and compound heterozygous mutations have been linked to severe neurodevelopmental phenotypes that often include microcephaly. Microcephaly is a condition where the brain does not develop properly, resulting in a smaller head circumference[28]. This can cause impaired cognitive development, slowed speech and motor functions, seizures, balance issues and other neurological problems in patients. Several novel VARS variants have recently been identified in patients displaying microcephaly, which was also linked to early-onset epilepsy[23]. The families of these patients are largely consanguineous, where VARS had previously been identified as a candidate 'disease gene'[29]. The identified variants are dispersed throughout the VARS coding sequence, many of which were predicted by comparison to *T. thermophilus* VARS to affect aminoacylation substrate recognition or protein structure. Though modeling in zebrafish and yeast

complementation assays indicate that the underlying mechanisms of these mutations are likely a decrease of protein function, that has yet to be tested explicitly[30].

1.1.3 Threonyl-tRNA Synthetase

Threonyl-tRNA synthetase (TARS) is a class II ARS that charges threonine (Thr) onto $tRNA^{Thr}$ [31]. Like most class II synthetases, TARS functions as a dimer. Each monomer has 4 domains: 2 N-terminal domains, the catalytic domain, and the anticodon binding domain[31]. The catalytic core of the enzyme contains the active site that is responsible for the recognition of Thr and ATP, the synthesis of the adenylate intermediate, and the transfer of the charged amino acid to $tRNA^{Thr}$. Zinc serves as a cofactor for TARS, and is found near its ATP binding site[32]. This ion is coordinated by a water molecule and three residues of the protein, and is necessary for TARS function[31,32]. The positive charge of the Zinc ion allows it to interact with hydroxyl groups of amino acids, which allows TARS to distinguish between the Thr and Valine (Val), which are structurally similar but differ in a hydroxyl group. The N2 domain of TARS is involved in the hydrolysis of erroneously aminoacylated Ser-$tRNA^{Thr}$ complexes as a part of TARS' 'fine sieve' post-transfer editing mechanism[15,32,33].

In addition to this editing function, TARS is one of the several ARS that have been related to angiogenesis, which is the process of blood vessel growth from the existing vascular network[34,35]. TARS is secreted out of the cell via an unknown mechanism to stimulate angiogenic extracellular signaling events[34]. Chicken embryos treated with exogenous TARS display expanded vasculature in chorioallantoic membrane assays, and application of TARS inhibitors in both zebrafish and endothelial cell tube formation assays

decrease cell migration, supporting the pro-angiogenic effects of TARS[34,36]. This secondary function in angiogenesis likely plays a role in the association between ARS and tumor progression, as inducing angiogenesis is one of the hallmarks of cancer[37].

1.2 Enzyme Kinetics

1.2.1 Enzyme Kinetics

Enzymes are essential for life, and thus it is important for us to understand them and the rates at which they work. Enzyme kinetics seeks to understand the affinities that substrates have for their enzymes and the maximum reaction rate that an enzyme can achieve[38]. In 1913, Leonor Michaelis and Maud Menten hypothesized that there was a general theory of enzyme rates, with several assumptions. They assumed that enzyme (E) and substrate (S) reversibly associate in forming an enzyme substrate complex (ES), which then forms product (P) in the second step of reaction, as shown in the equation:

$$E + S \underset{k_{-1}}{\overset{k_1}{\rightleftharpoons}} ES \xrightarrow{k_2} E + P$$

Next, the steady-state assumption assumes that [ES] reaches and stays at a constant value in this system, meaning that ES is formed at a rate equal to the sum of ES dissociating to E+S and ES being converted into E+P. Finally, Michaelis-Menten kinetics assumes that the rate of back reaction (k_{-2}) is small relative to the rate of the reaction catalyzed by the enzyme (k_2) (because enzymes can catalyze both the forward and reverse reactions). To account for this we measure initial reaction velocities, where the enzyme has maximum substrate concentrations and no product, minimizing the back reaction. This results in the Michaelis-Menten equation:

$$v = \frac{V_{max}[S]}{k_m + [S]}$$

In this equation V_{max} is the maximum velocity that can be reached by a certain concentration of enzyme at saturating enzyme conditions, v is the reaction velocity and K_m is the substrate concentration at ½ of the reaction's V_{max}. K_m is approximately inversely related to the affinity that a substrate has for its enzyme, depending on the rates of ES association (k_1) and dissociation (k_{-1}), and the rate of E+P formation (k_2) according to the following equation:

$$k_m = \frac{k_{-1} + k_2}{k_1}$$

The Michaelis-Menten equation can be represented graphically with a Michaelis-Menton plot, with [S] on the x-axis and v on the y-axis (Figure 2)

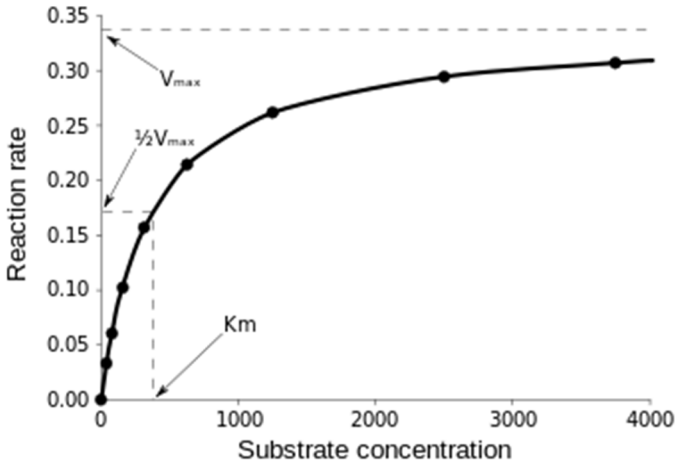

Figure 2. An example Michaelis-Menten plot showing V_{max}, K_m, v, and [S][39].

Because of the fact that the V_{max} value for a Michaelis-Menten plot depends on the experimental enzyme concentration V_{max} is often converted to the enzyme's turnover number (k_{cat}), which is the number of substrate molecules converted into product per enzyme over time[38]. Experimentally, a Michaelis-Menten plot is derived from many

individual progress curves. By plotting product produced over time in a progress curve and taking the slope from that curve (v), we can use this data as an individual point in our Michaelis-Menten curve. After making many progress curves at many different substrate concentrations, we can combine them to make the curve.

Adding inhibitors to the Michaelis-Menten reaction conditions can change the apparent V_{max} and K_m values for the reaction depending on the type of inhibitor added (Table 1).

Table 1. The four main types of inhibitors, their effects on the V_{max} and K_m values of a Michaelis-Menten Plot, and the explanation for their effects[38].

Type of Inhibitor	Effect on V_{max}	Effect on K_m	Explanation
Competitive	None	Increased	Though the inhibitor will bind and inhibit its substrate, increasing substrate concentration will prevent it will outcompete it. This means that with enough substrate the enzyme can still reach Vmax, resulting in an increased K_m apparent.
Pure non-competitive (Inhibitor binding doesn't change substrate binding)	Decrease	None	Non-competitive inhibitors will lower the number of enzyme molecules available to perform the reaction (lowering V_{max}) without changing the enzyme's affinity for its substrate (K_m)
Mixed non-competitive (Inhibitor may preferentially bind the E or ES complex)	Decrease	May decrease K_m	Depending on the inhibitor's affinity for the E or ES complexes, K_m may decrease. Mixed inhibitors will lower V_{max} by lowering the amount of active enzyme.
Uncompetitive	Decreased	Decreased	Since uncompetitive inhibitors only interact with the ES complex, this increases the enzyme's affinity for substrate through LeChatlier's principle (decreasing K_m). V_{max} is also decreased because IES complex formation

			does not lead to product formation.

Using a combination of kinetic and structural data for a given enzyme, one could discern the type of inhibition that a particular inhibitor exerts on its target enzyme[40]. In addition to classification based on their mechanism of interacting with their target enzymes, some inhibitors are also classified by their time-dependence or the binding strength of the inhibitor[41]. Slow binding inhibitors bind or dissociate from their target enzymes slowly, complicating the process of determining the affinity of the inhibitor for its target enzyme. There are several different mechanisms of slow binding inhibition aside from the classic reversible mechanism of[41]:

$$E + I \underset{k_4}{\overset{k_3}{\rightleftharpoons}} EI$$

A slow binding inhibitor can act through an induced fit mechanism, where it will form an initial binary complex (governed by the rates k_3 and k_4) before the enzyme undergoes a far slower isomerization step, as shown below[41]:

$$E + I \underset{k_4}{\overset{k_3}{\rightleftharpoons}} EI \underset{k_6}{\overset{k_5}{\rightleftharpoons}} EI^*$$

Slow binding inhibitors can also act through mechanisms of conformational selection, where either the enzyme or the inhibitor will isomerize between multiple forms in solution, and only one of these isomers will interact with its binding partner. In these cases, the slow isomerization limits the rapid formation of the EI complex. Only the mechanism for

enzyme isomerization is shown, because small molecule inhibitors do not often undergo this isomerization[41].

$$E \underset{k_8}{\overset{k_7}{\rightleftharpoons}} E^* \underset{k_{10}}{\overset{k_9}{\rightleftharpoons}} E^*I$$

Because it takes time for the free and bound versions of the inhibitor to reach an equilibrium, progress curves of slow binding inhibitors can display two different velocities. These velocities are v_i, the initial velocity of the reaction before the inhibitor starts to interact with the enzyme (which is identical to that of the uninhibited reaction), and v_s, the steady state velocity after the free and bound inhibitor states have reached equilibrium (Figure 3).

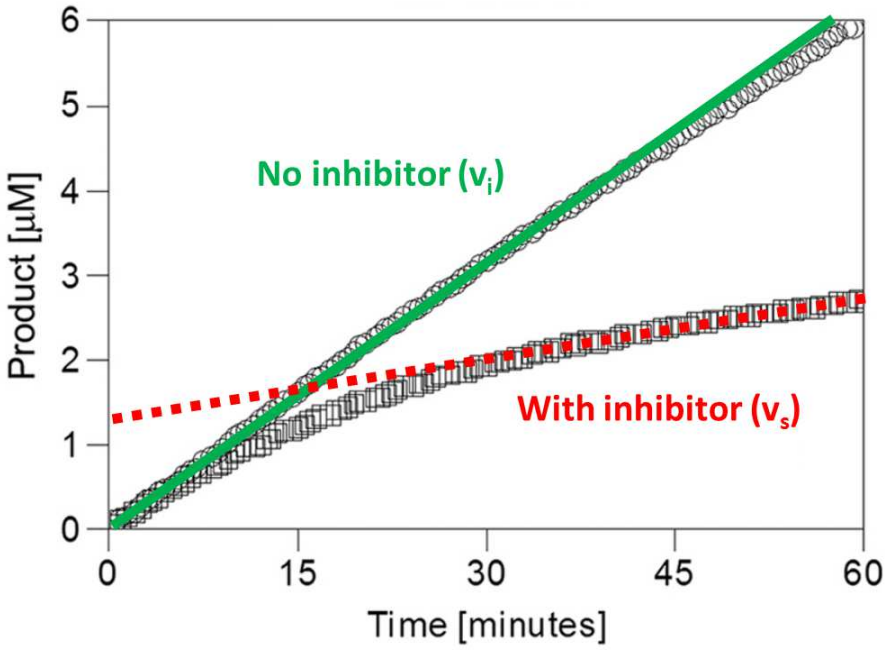

Figure 3. The effects of a slow binding inhibitor on a progress curve. Two progress curves, one without an inhibitor and one with a slow binding inhibitor. The two slopes of the slow binding inhibitor curve are labeled as v_i and v_s.

To combat this, when collecting experimental progress curve data researchers can pre-incubate the enzyme with the inhibitor prior to adding other reaction reagents. This will only work for some inhibitor types and needs to be done in the absence of substrate in the case of competitive inhibitors.

Some inhibitors bind to their target enzyme with such an affinity that the assumptions used to calculate K_i values are no longer valid[41]. Such affinity is usually the result of having very slow dissociation rates for the EI complex. Slow binding inhibitors are often tight binding inhibitors as well. In these cases, the inhibitor will display a slow rate of association for the E+I complex (k_{on}), but an even slower dissociation rate (k_{off}) from the E+I complex. This allows the inhibitor to have a high affinity for its target enzyme despite having a very slow rate of association[41].

1.2.2 Inhibitors of Threonyl-tRNA Synthetase

There are several known inhibitors of TARS. Borrelidin is a macrolide-polyketide, a large cyclic 18-membered lactone ring (Figure 4).

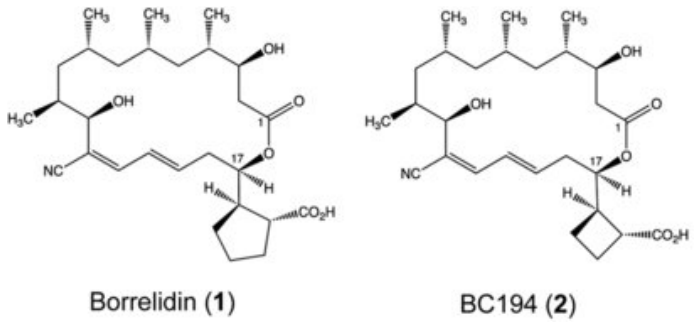

Figure 4. The Structure of two TARS inhibitors, Borrelidin and the Borrelidin Derivative BC194 [42].

Produced by *Streptomyces rocheii*, borrelidin has been shown having anti-malarial, anti-angiogenic, anti-fungal, and anti-tumor effects, in addition to inhibitory effects on TARS[43–

[47]. Borrelidin is a slow, tight binding inhibitor of TARS that displays non-competitive mechanisms of interaction, and will severely denature the enzyme over time[40,48]. This means that borrelidin inhibits TARS more the longer they're incubated together, and that once bound it has a low rate of dissociation from the enzyme. Borrelidin binds close to the zinc ion in the active site of *E. coli* TARS, interacting with Thr-307, His-309, Cys-334, Pro-335, Leu-489, and Leu-493[40]. Because of its inhibitory effects on TARS, borrelidin has undesired cytotoxic effects. BC194 is a borrelidin derivative that exhibits decreased cellular toxicity compared to that of borrelidin[42]. BC194 has a 4-membered carbon ring at carbon 17 instead of the 5-membered ring seen in borrelidin (Figure 4).

Obafluorin is a β-lactone, first isolated from *Pseudomonas fluorescens* in 1984[49,50] (Figure 5).

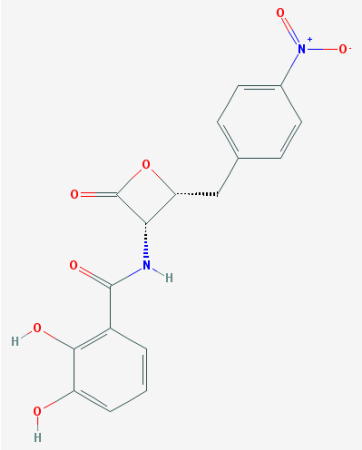

Figure 5. The Chemical Structure of the TARS Inhibitor Obafluorin.[51]

Obafluorin exhibits antibacterial activity against a range of bacteria, including *Staphylococcus aureus, E. coli,* and *Enterobacter cloacae*[49]. Despite being a β-lactone, obafluorin exhibits relative susceptibility to hydrolysis via β-lactamases and is sensitive to

acidic conditions, which may indicate its instability compared to other β-lactones[49,52]. Obafluorin was recently hypothesized to be an inhibitor of TARS and has not yet been kinetically characterized[52]. A recent analysis of the obafluorin synthesis gene cluster reveals a gene coding for a TARS paralog, ObaO (unpublished data from the Wilkinson lab). This paralog may serve as a means of conferring obafluorin resistance to *Pseudomoas fluorescens*, if it is not susceptible to TARS inhibition. ObaO differs from wild-type TARS in a single cysteine (Cys) residue in its active site, which is substituted for a Val residue in ObaO. This may indicate where obafluorin interacts with TARS and its mechanism of inhibition. EHTS-1, a benzoate analog of obafluorin, may have inhibitory effects on TARS like those hypothesized about obafluorin.

1.3 Aminoacylation as a Means of Post-Translational Modification

1.3.1 Post-Translational Modification Can Affect Protein Function

Proteins perform most of the processes that occur both intracellularly and extracellularly in organisms. Though the diversity of the proteome and the protein functions found throughout the proteome is large, the number of protein coding genes is noticeably smaller[53]. This is accomplished through several different mechanisms ranging from alternate promoter sequences and alternative splicing at the level of mRNA to post-translational modification (PTM) at the level of protein. PTM is the covalent modification of amino acid side chains or peptide linkages in a protein, and there are hundreds of different PTMs that can occur across the proteome. PTMs can have many different effects on a protein depending on both the target protein and the modification, as well as the organism that the modification is occurring in, as the systems for PTM of

proteins are slightly different between prokaryotes and eukaryotes[53,54]. These effects include but aren't limited to changing the conformation of a protein, creating docking sites for other proteins, changing the catalytic efficiency of an enzymatic protein, or changing a protein's cellular localization. PTMs are generally reversible, which is important in the context of cellular signaling. A reversible PTM is more likely to be able to change on a shorter time-frame and thus be more sensitive to cellular conditions than an irreversible PTM or just protein levels in general, which would require protein synthesis, degradation or re-localization to alter the signal that the protein is propagating. PTMs like the proteolysis of peptide bonds in converting apoenzymes to holoenzymes are irreversible, and thus are likely slower to respond to the changing cellular environment than reversible PTMs like phosphorylation, acetylation, or ubiquitination[53]. Though this reversibility is important in the context of cellular signaling, it can also make it difficult to detect PTMs via methods like x-ray crystallography or mass spectrometry. To prevent deacetylation or removal of similar post-translational modifications of proteins experimentally, we could minimize sirtuin activity via sirtuin inhibitors like EX-527 or sirtinol[55,56].

1.3.2 Aminoacylation of Proteins

In 1997, Sylvie Gillet demonstrated that *E. coli* Methionyl Aminoacyl-tRNA Synthetase (MetRS) could auto-aminoacylate[57]. This occurs via a covalent isopeptide bond forming between the carboxylate of the amino acid and the ε-NH_2 group of a lysine residue. This modification lowered the enzyme's ability to perform both ATP isotopic exchange and to aminoacylate $tRNA^{Met}$. Since then, other authors have demonstrated that

other ARS and ARS paralogs, like *Bacillus stearothermophilus* MetRS and an *Escherichia coli* lysyl aminoacyl-tRNA synthetase (KARS) paralog, are capable of aminoacylating other proteins (the KARS paralog is only known to aminoacylate *E. coli*. elongation factor P) by the same mechanism of isopeptide bond formation with the ε-NH_2 group of a lysine residue discussed in Gillet's 1997 paper[57–59].

In 2017, He et al. published NMR and mass spectrometry data detailing that all twenty amino acids were identified as modifiers of lysine residues, using a documented multi-specific amidase[60,61]. This suggested that the implications of the previous work in protein aminoacylation were broader than expected, that all of the ARS are capable of aminoacylating the ε-NH_2 group of lysine residues, and that the modifications can be removed by deacetylases like Sirtuin1 or Sirtuin3 via the normal deacetylation mechanism[60]. Aminoacylation of proteins by ARS may represent a novel PTM that is directly sensitive to amino acid levels and thus could be used as a mechanism for amino acid sensing.

1.4 Autophagy

1.4.1 Overview of Autophagy

Autophagy is a process of cellular recycling, where macromolecules in the cell are degraded to their fundamental parts[62,63]. There are several different subtypes of autophagy, which are either selective (removing unnecessary or harmful materials from the cell) or bulk (recycling cellular materials for the purpose of maintaining amino acid, lipid, and nucleotide level homeostasis, triggered by starvation conditions) autophagy[62]. There are three subtypes of autophagy: macroautophagy – the breaking down of damaged

cell organelles or unused proteins, microautophagy – the direct and largely random engulfment of cytoplasmic material into a lysosome, and chaperone-mediated autophagy – the recognition and selection of cytosolic proteins that are then sent to lysosomes for degradation[62,64,65]. Here, the term autophagy is used to refer to the process of macroautophagy.

Autophagy is generally regulated by the ATG genes, over 30 of which have been described[66]. These generally display distinct similarity across human and yeast genomes. Autophagy begins with the construction of a vesicle precursor membrane called the preautophagosome (PAS), which will grow and start to isolate macromolecules in the cytoplasm as the structure becomes an autophagosome[62,66,67] (Figure 6). This autophagosome will then fuse with a lysosome, which contains enzymes that facilitate the degradation of the contents of the autophagosome, thus facilitating the breakdown and recycling of cellular constituents to their basic metabolites.

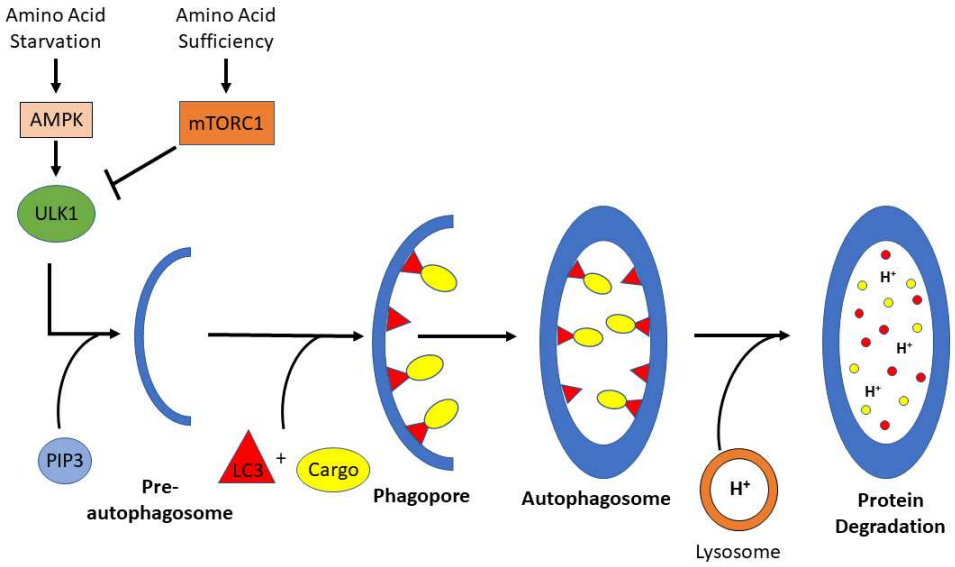

Figure 6. A visual representation of the autophagy pathway.

Under starvation conditions, AMPK activates ULK1, which begins the nucleation of inositol-modified membrane components into the PAS through ULK1 phosphorylating ATG13 and VSP34 in the PI3 kinase complex. In this step, phosphatidylinositol 3-phosphate (PIP3) is added to the PAS. This structure is then elongated by incorporating additional material to generate a phagopore/isolation membrane. During this step, 1A/1B light chain 3b (LC3) conjugated to phosphatidyl ethanolamine is incorporated into the structure along with the ATG12-ATG5-ATG16L1 complex, which assists in the conjugation of LC3 to phosphatidyl ethanolamine (PE)[66]. As macromolecules start to become isolated by the growing phagophore, the generally non-selective cargo of the soon-to-be autophagosome are tagged with poly-ubiquitin chains that are selective for autophagy and are conjugated to LC3s with the help of autophagy receptor and adaptor proteins[66,68,69]. The autophagosome is then fully extended to complete the double walled vesicular structure that is the autophagosome.

Under conditions of amino acid sufficiency, mTORC1 (mammalian target of rapamycin complex 1) (a protein complex containing the serine/Thr kinase mammalian target of rapamycin) will phosphorylate and inhibit ULK1. mTORC1 is typically thought of as one of the key regulators in the initiation of autophagy due to its relationship with ULK1 and amino acid sensing. Despite this, it is poorly understood how mTORC1 reacts to amino acid levels[70]. Currently, mTORC1 is only known to sense leucine and arginine levels, but is not activated when deprived of the other 18 amino acids[71]. Analysis of recent mass spectrometry data suggests that many components of the autophagy machinery may interact with and are aminoacylated by various ARS[60,72]. For example,

TARS, VARS and LARS have been suggested to aminoacylate ATG101 from the ULK1 complex, AMPK, and PI3 kinase. If these modifications had an effect on autophagy levels, they would provide a rapid and direct means for the autophagy pathway to sense the amino acid pool, as well as fill in the current gap in our knowledge of how mTORC1 serves as the amino acid sensor for the autophagy pathway.

1.4.2 Autophagy in Disease

Due to autophagy's intrinsic link to the degradation of proteins and the accumulation of macromolecules in the cell, autophagy and proteins related to the autophagy pathway have been implicated in several different diseases[66,73]. These range from neurodegenerative diseases like Crohn's disease and Alzheimer's disease to diabetes[66].

Crohn's disease has been linked to duplications in the IRGM gene, which is involved in the initiation of autophagy[74,75]. In addition, a single nucleotide polymorphism in ATG16L1, a protein that mediates the conjugation of PE to LC3 in autophagy's response to pathogens, has also been associated with Crohn's disease[76–78]. Several downregulating variants in the ATG7 gene promoter, which regulates the expression of a key protein in autophagosome formation, have been identified in patients with Parkinson's disease[79]. An upregulating variant in the ATG5 gene promoter has also been identified in a patient with Parkinson's disease[80]. Problems in the *presenilin* genes are the most common cause of familial Alzheimer's disease[81]. Deficiency in presenilin1 has been linked to the improper translocation of the V0a1 subunit of the H^+-ATPase proton pump, resulting in improper acidification of the lysosome and in turn abnormal autophagy. Finally, autophagy has been

implicated in type 2 diabetes mellitus and the accumulation of human islet amyloid polypeptide in pancreatic β cells, which cause functional impairment and loss of β cells[66].

In addition to this, the autophagy pathway and its proteins have been demonstrated as having both tumor suppressive and tumor proliferative effects depending on the phase of tumorigenesis[82]. Autophagy upregulation can provide established tumors decreased sensitivity to normally fatal environmental stimuli and can confer starvation resistance. This aids in tumor progression, particularly in tumors undergoing the mesenchymal to endothelial transition (MET)[82,83]. On the other hand, *Becn1*$^{+/-}$ mice (*Becn1*$^{-/-}$ mice are fatal) can spontaneously develop several different types of malignancies[82,84,85]. The tumor suppressive properties of autophagy in the early phases of tumorigenesis have several possible mechanisms, including: suppression of reactive oxygen species (which have genotoxic effects), destroying micronuclei (which arise in conditions of cell-cycle perturbation), and controlling the levels of ras homology family member A (which is involved in cytokinesis)[82].

1.5 Thesis Objectives

Here we demonstrate the specific autoaminoacylation activity of both *E. coli* and human TARS, as well as *E. coli* histidyl aminoacyl-tRNA synthetase (HARS) using procedures modified from Yanasigawa et al., 2010[59]. These reactions were ATP dependent, and in the cases of the TARS enzymes were inhibited by $tRNA^{Thr}$ and the TARS inhibitors obafluorin and BC194. Here we also demonstrate the inhibitory effects of obafluorin on both *E. coli* and human TARS activity and determine an IC50 value for each enzyme.

CHAPTER 2: EXPERIMENTAL PROCEDURES AND MATERIALS

2.1 Protein Purification

The assays that comprise the body of this thesis utilize purified ARS enzymes, which were overexpressed in *E. coli* and purified using an ÄKTA purification system as described in previous publications[86–88]. All purified proteins were expressed in pET vectors and transformed into Veggie BL21(DE3) Competent Cells (Millipore) or NovaBlue (Millipore) *E. coli* cells. Cells were grown in luria broth from stocks kept at -80°C and expression of our target proteins was induced with isopropyl β-D-1-thiogalactopyranoside (IPTG) at an OD600 of between 0.4-0.6 A. All our proteins were His tagged, and thus were purified using a HisTrap HP 5 mL nickel-affinity column (GE Healthcare) on an ÄKTA purifier system (GE Healthcare). Following purification, our samples were dialyzed with SnakeSkin 10K MWCO Dialysis tubing (Thermo Scientific), concentrated using Amicon Ultra 15 centrifugal filters (Millipore) and had their concentrations determined using a Nano-Drop spectrophotometer system.

2.2 In vivo $tRNA^{Thr}$ Transcription and Purification

To obtain purified $tRNA^{Thr}$ for our kinetics and aminoacylation assays, $tRNA^{Thr}$ was overexpressed in *E. coli* and purified by gel electrophoresis and electrolution as described in previous works from the Francklyn Lab[89,90]. E. *coli* $tRNA^{Thr}$ was expressed in BL21 *E. coli* cells, and purified via phenol chloroform extraction. The $tRNA^{Thr}$ was then precipitated overnight in 2.5x volume ethanol and 0.1x volume sodium acetate and subjected to centrifugation. After washing the pellet with 75% ethanol, the pellet was

resuspended in 10 mM HEPES pH 6. This sample was then mixed with 6X blue loading dye and loaded into a large urea gel (6.5% polyacrylamide (19:1 acrylamide:bisacrylamide), 8 M urea, and 0.5 M sodium acetate pH 5). The gel was run at 50 watts until the dye front almost ran off the gel, at which point the gel was imaged via a UV light box and the $tRNA^{Thr}$ band was identified. This band was excised, chopped and placed into an electroeluter apparatus (Whatman/Schleicher & Schuell) overnight. After electroelution, the purified sample was again precipitated with 2.5x volume ethanol and 0.5x volume sodium acetate and then resuspended in TE6 buffer.

2.3 ARS Kinetics Assay

To measure the effects of obafluorin on TARS' canonical tRNA charging activity, an assay modified from Ruan et al., 2005 was used, where active enzyme was incubated with its necessary substrates and its activity measured ^{14}C labeled Thr and a liquid scintillation counter[40]. Purified TARS protein (10 nM) was pre-incubated with varying concentrations of obafluorin for 10 minutes. After pre-incubation, TARS and obafluorin were added to a master reaction mixture with the final concentrations of 100 mM HEPES pH 7, 4 mM ATP, 10 mM $MgCl_2$, 50 µM ^{14}C labeled Thr (Moravek), and 5 µM $tRNA^{Thr}$. This mixture was then incubated for 10 minutes, with time points being taken at 1, 2.5, 5, and 10 minutes. At each time point, three 5 µl aliquots were spotted onto 5% TCA presoaked 3MM Whatman paper (Sigma-Aldrich). After letting the spots dry, the Whatman paper was washed three times with 5% TCA, and once with 95% ethanol. Whatman paper was dried and the counts on each square of paper analyzed with

a liquid scintillation counter using Hydrofluor Liquid Scintillation Fluid (National Diagnostics).

2.4 Autoaminoacylation Assay

To measure levels of ARS autoaminoacylation, enzyme was incubated with its necessary substrates in a protocol modified from Yanasigawa et al., 2010, and was visualized the reaction via gel electrophoresis and autoradiography (autorad)[59]. Purified TARS (10 μM) was combined with 50 mM Tris HCL pH 7.5, 50 μM ^{14}C labeled Thr (Moravek), 4 mM ATP, 10 mM $MgCl_2$, 5 mM βME, and 5 μg/mL pyrophosphatase (Thermo Scientific). This mixture was incubated in a 37˚C water bath for 2-6 hours, with time points taken at key intervals. These time points were quenched in 4X SDS PAGE sample buffer (200 mM Tris pH 6, 4% SDS, 4 mg/mL bromphenol, 4% βME, 40% glycerol, and 0.004% pyronin Y) and then run on an 8% SDS PAGE gel. This gel was fixed in a 50% methanol/10% acetic acid solution for 20 minutes and then dried in a 40% glycerol/10% ethanol solution for 30 minutes. This dry gel was then imaged by exposing a kodak phosphor screen (BioRad) to the gel for 62 hours and developing the screen on a Pharos FX phosphoimager system (BioRad). Results were quantified using the volume analysis tools in QuantityOne (BioRad).

CHAPTER 3: AUTOAMINOACYLATION OF AMYINOACYL-TRNA SYNTHETASES

3.1 Introduction

The current hypothesis of how ARSs could serve as a mechanism of sensing amino acid levels in the autophagy pathway relies on ARSs being able to aminoacylate proteins. This was already demonstrated in He et al., 2017, but has yet to be individually validated for both TARS and HARS[60]. Among the many targets of each enzyme identified in He et al., 2017, both TARS and HARS aminoacylate themselves, making themselves the easiest targets to use to validate this function. Using an autoaminoacylation procedure modified from Yanasigawa et al., 2010, the autoaminoacylation abilities of several different ARSs were tested in various conditions, addressing the substrates necessary for the reaction and the effects of tRNA on the reaction.

3.2 *E. coli* ARS Results

To validate the requirements for the *E. coli* TARS' protein aminoacylation reaction, autoaminoacylation assays were performed with varying concentrations of enzyme, Mg^{2+}, and ATP. These assays revealed that the reaction is dependent on the presence of ATP, and is sensitive to Mg^{2+} concentrations. (Figure 7).

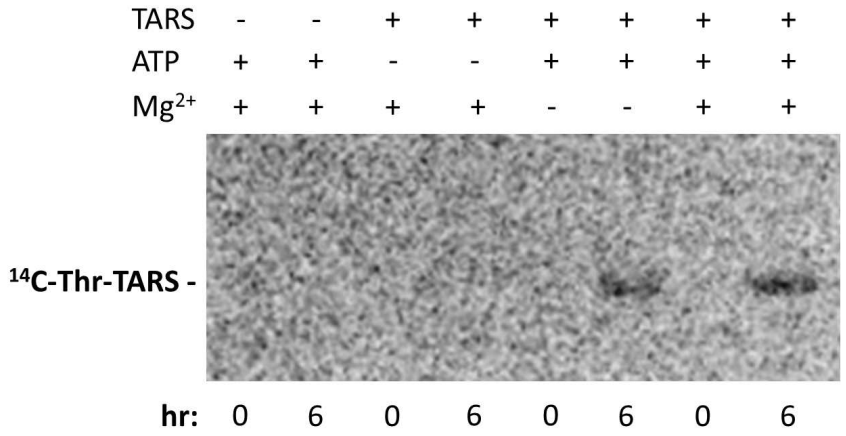

Figure 7. *E. coli* TARS is capable of autoaminoacylation. N = 2 An autoradiograph showing *E. coli* TARS autoaminoacylation at 0 and 6 hours varying (from left to right) enzyme concentration (0 or 10 μM), ATP concentration (0 or 4 mM) and Mg^{2+} concentration (0 or 10 mM).

Though there was no $MgCl_2$ added to the reaction mixture for the 'No $MgCl_2$' condition, we did not test whether the reaction would occur with no Mg^{2+} present (for example ensuring that there is no Mg^{2+} in our ATP salt), and thus cannot say whether the reaction can occur without Mg^{2+}.

Following this, we were interested in the time frame of this reaction. To test this, we performed an autoaminoacylation assay, taking time points at 0, 0.25, 0.5, 1, 2, 3, 4, and 6 hours (Figure 8a). Graphing this autorad data reveals that the reaction reaches its peak progress at 2 hours (Figure 8b). Following this, levels of aminoacylated TARS decrease and eventually plateau around 4 hours.

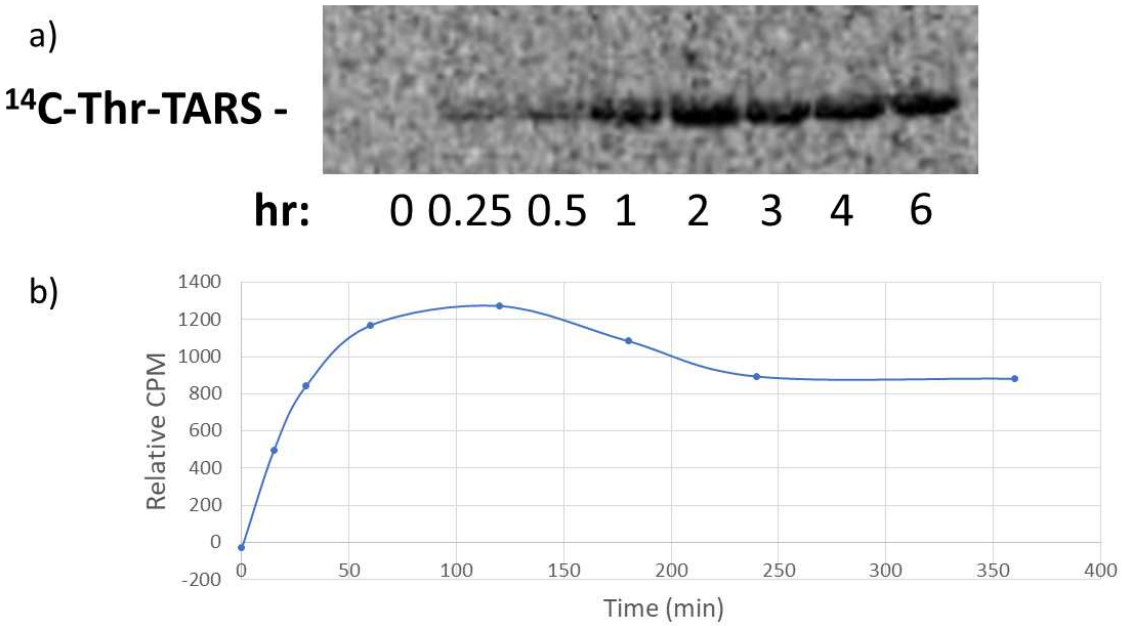

Figure 8. The time frame of the *E. coli* TARS autoaminoacylation reaction. N = 2. a) An autoradiograph showing eight time-points (increasing left to right) taken at during an *E. coli* TARS autoaminoacylation assay. **b)** A progress curve for a six-hour long E. coli TARS autoaminoacylation assay in units of autorad detected radiation (U).

With a better understanding of the kinetics of the reaction, we next wanted to see the effects of increasing $tRNA^{Thr}$ concentration on the rate of the aminoacylation reaction. Adding 10 µM $tRNA^{Thr}$ to an autoaminoacylation assay resulted in decreased *E. coli* TARS autoaminoacylation (Figure 9a). Again, graphing this autorad data reveals that $tRNA^{Thr}$ greatly decreases the autoaminoacylation effects of *E. coli* TARS (Figure 9b).

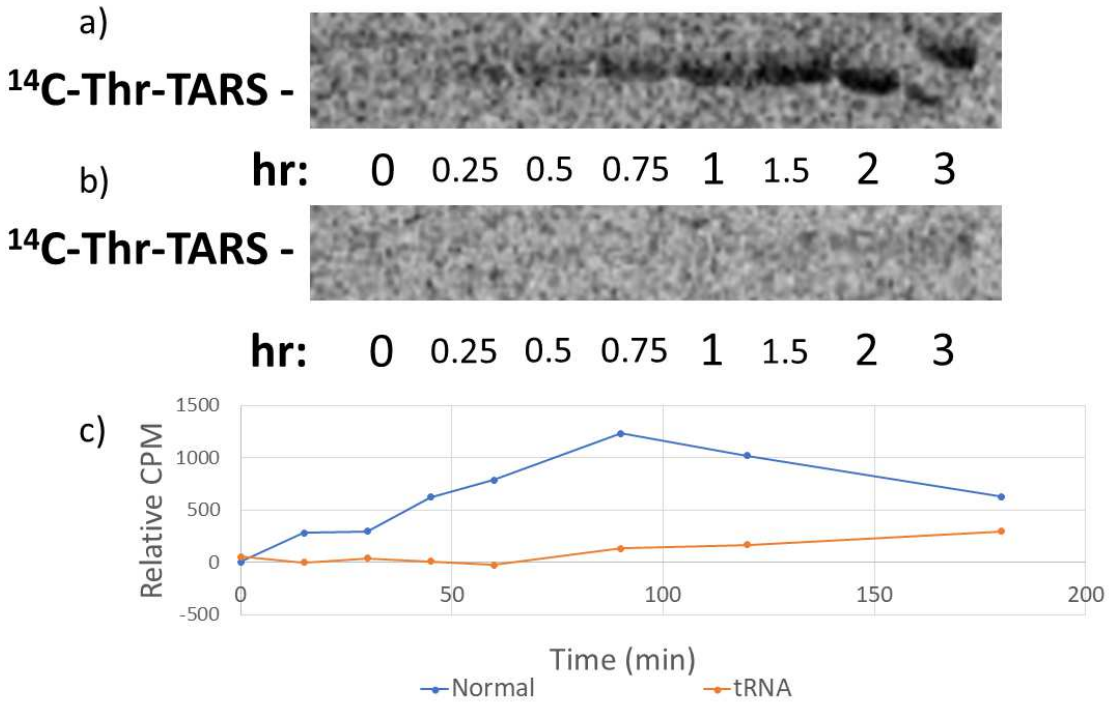

Figure 9. $tRNA^{Thr}$ decreases E. coli TARS autoaminoacylation. N=1

a) An autoradiograph showing eight timepoints (increasing left to right) of a three-hour long autoaminoacylation assay without tRNA. **b)** An autoradiograph showing eight timepoints (increasing left to right) of a three-hour long autoaminoacylation assay with 10 µM tRNA. **c)** Two *E. coli* TARS autoaminoacylation progress curves, one with 10 µM tRNA, and one without, shown in units of autorad detected radiation (U).

Finally, the specificity of the *E. coli* TARS autoaminoacylation reaction was tested. To test this, two side by side aminoacylation assays were run, one with TARS and Thr, and the other with TARS and His. This assay revealed that the reaction is in fact Thr specific, as there are only bands in the autorad in the timepoints that contain Thr (Figure 10).

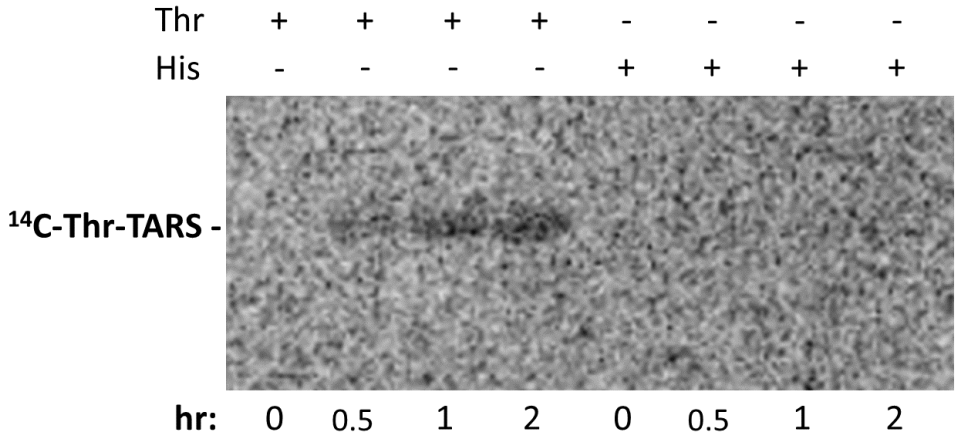

Figure 10. E. coli TARS autoaminoacylation is Thr specific. N=1. An autoradiograph with two *E. coli* TARS autoaminoacylation assays, one (the left four lanes) with Thr (50 μM), the other (the right four lanes) with His (50 μM).

After finding the requirements for *E. coli* TARS' autoaminoacylation reaction and confirming its specificity, *E. coli* HARS was tested to confirm the requirements for its autoaminoacylation reaction. To test this, an autoaminoacylation assay with available *E. coli* HARS was performed, varying concentrations of ATP. As anticipated, E. coli HARS was also capable of autoaminoacylation, and like autoaminoacylation of *E. coli* TARS, autoaminoacylation of *E. coli* HARS is also ATP dependent (Figure 11a). The specificity of the HARS autoaminoacylation reaction was also tested via two side by side autoaminoacylation reactions, one with His and the other with Thr. This showed that, like *E. coli* TARS, *E. coli* HARS protein aminoacylation activity is specific to its cognate amino acid (Figure 11b).

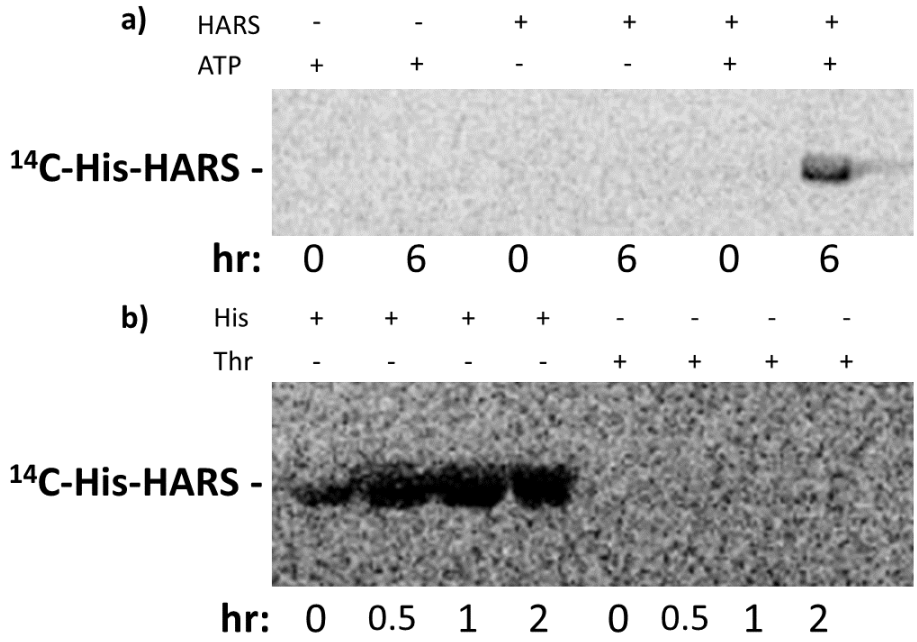

Figure 11. E. coli HARS is capable of specific autoaminoacylation with His. a) An autoradiograph showing *E. coli* HARS autoaminoacylation at 0 and 6 hours varying (from left to right) enzyme concentration (0 or 10 μM) and ATP concentration (0 or 4 mM). **b)** An autoradiograph with two *E. coli* HARS autoaminoacylation assays, one (the left four lanes) with His (50 μM), the other (the right four lanes) with Thr (50 μM).

This set of experiments supported that both *E. coli* TARS and *E. coli* HARS are capable of autoaminoacylation. These reactions have a reproducible time frame and are both cognate amino acid specific and ATP dependent, likely occurring through the same mechanism undergone in the aminoacylation of their cognate tRNA molecules.

3.3 Human TARS Results

To validate human TARS' protein aminoacylation abilities and the conditions under which it autoaminoacylates, autoaminoacylation assays were performed with varying concentrations of Mg^{2+}, and ATP. These assays did support human TARS being able to autoaminoacylate, though there was some protein aggregation (Figure 12).

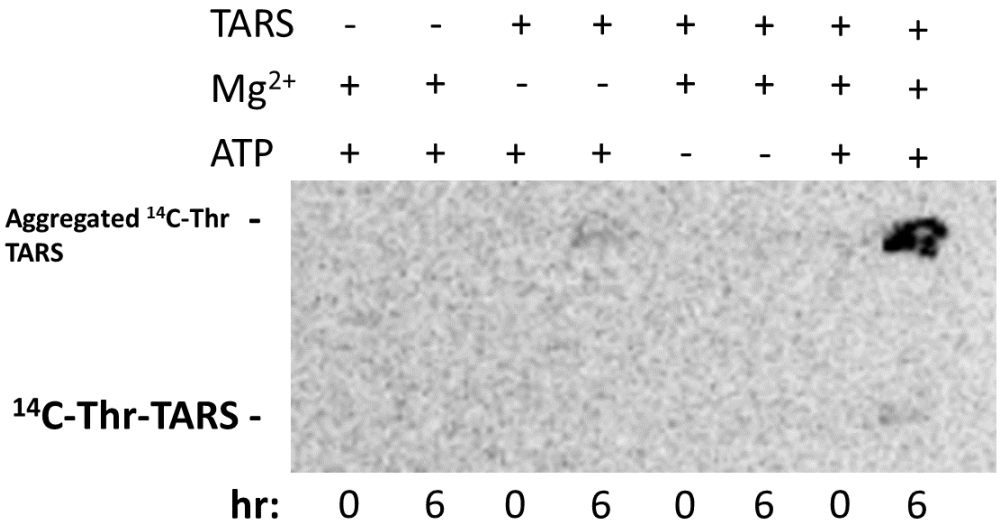

Figure 12. Human TARS is capable of autoaminoacylation. N=3. An autoradiograph showing human TARS autoaminoacylation at 0 and 6 hours varying (from left to right) enzyme concentration (0 or 13 μM), Mg^{2+} concentration (0 or 10 mM) and ATP concentration (0 or 4 mM).

Rather than showing up as a strong band at the molecular weight of human TARS (75 kDa), there are strong bands barely in the very top of the gel, and a faint band at 75 kDa. These results showed up consistently across all three of these experiments, and were not fixed with increased reducing agent or increased time denaturing at 90°C before SDS PAGE.

Regardless, the data show that human TARS autoaminoacylation is ATP dependent, and is sensitive to decreased Mg^{2+} concentrations. To test whether the TARS' autoaminoacylation abilities are specific to Thr, two side by side autoaminoacylation assays were run with human TARS, one with Thr and one with Val. This revealed that like protein aminoacylation by *E. coli* TARS, protein aminoacylation via human TARS is specific to Thr (Figure 13).

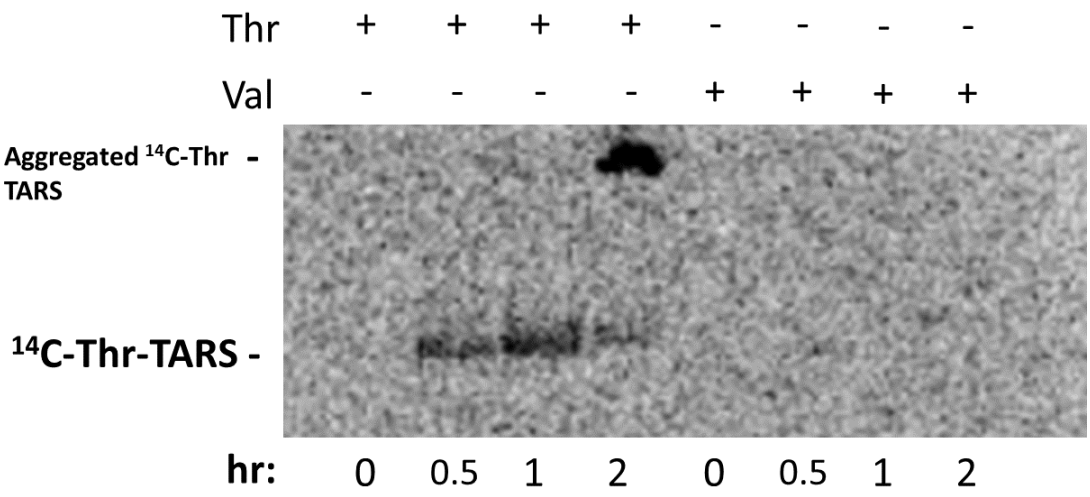

Figure 13. Human TARS autoaminoacylation is Thr specific. An autoradiograph with two human TARS autoaminoacylation assays, one (the left four lanes) with Thr (50 μM), the other (the right four lanes) with Val (50 μM).

These experiments also showed that the bands at the top of the autoradiograph are likely aggregates of human TARS and that their formation is likely time dependent. Next, we wanted to test the effects of $tRNA^{Thr}$ on human TARS autoaminoacylation, which we accomplished by running an aminoacylation assay with 10 μM $tRNA^{Thr}$ and comparing it to human TARS lanes without $tRNA^{Thr}$. Just like we see in E. coli TARS, the presence of $tRNA^{Thr}$ decreases TARS autoaminoacylation (Figure 14a). When counted via a volume analysis tool in QuantityOne, we see that the in the presence of $tRNA^{Thr}$, human TARS

autoaminoacylation only reaches 80% of that reached by the reaction without $tRNA^{Thr}$ present (Figure 14b). These experiments appeared to have less aggregated ^{14}C labeled TARS than previous experiments with the human enzyme. This may be due to increased mixing of the reaction reagents during its 2-hour incubation at 37°C.

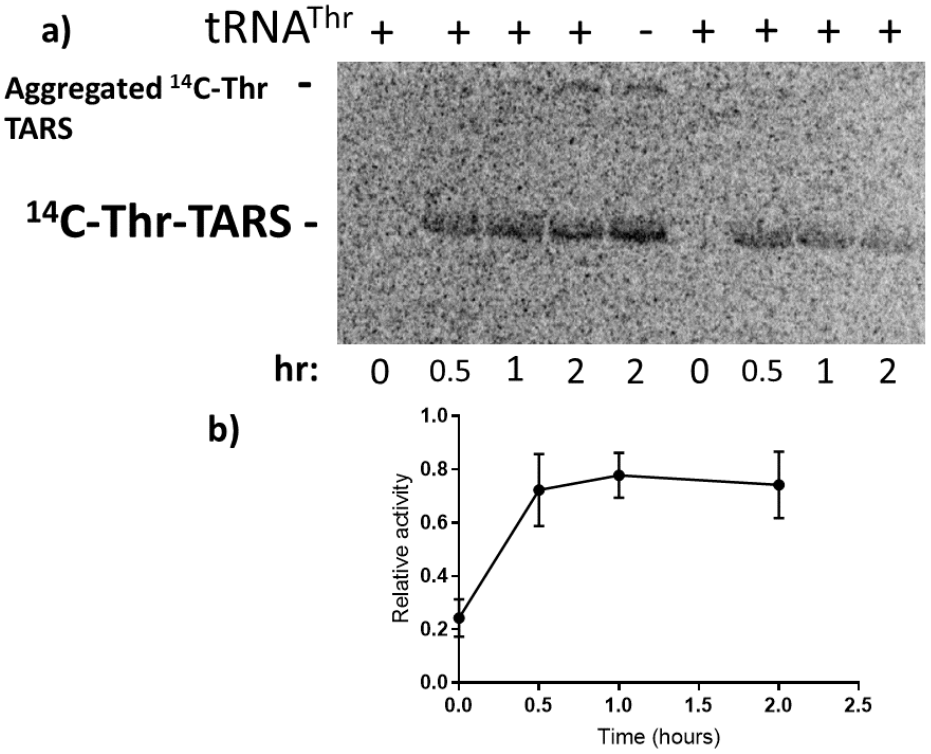

Figure 14. $tRNA^{Thr}$ decreases human TARS autoaminoacylation. N=3 a) An autoradiograph with three human TARS autoaminoacylation assays, one (the left four lanes, time increasing left to right) with $tRNA^{Thr}$ (15 µM), one (the center lane) with no tRNA, and the last (the right four lanes, time increasing left to right) with $tRNA^{Thr}$ (15 µM). **b)** The average progress curve of human TARS in the presence of $tRNA^{Thr}$ compiled from three autoaminoacylation assays. This curve is normalized to the activity of a human TARS autoaminoacylation assay without $tRNA^{Thr}$, incubated for two hours. Error bars represent the standard deviation for each time point.

From these experiments we confirmed that human TARS is capable of autoaminoacylation as published in He et al., 2017[60]. Like the bacterial enzyme, this reaction is both Thr specific and ATP dependent, but is more susceptible to protein aggregation in our assay than the bacterial enzyme. Autoaminoacylation of human TARS

is also decreased by $tRNA^{Thr}$. Human TARS' specificity to Thr, dependence on ATP, and susceptibility to increasing tRNA concentration all suggest that these reactions are likely occurring through the same mechanism of TARS' canonical function of $tRNA^{Thr}$ aminoacylation.

CHAPTER 4: CHARACTERIZING THE INHIBITORY EFFECTS OF OBAFLUORIN ON THREONYL-TRNA SYNTHETASE ORTHOLOGS.

4.1 Introduction

Obafluorin is a β-lactone with a nitrobenzene and an *ortho*-benzenediol on either side of the β-lactone[50]. β-lactams and β-lactones are known for their potential as antibiotics, due to the mechanism of penicillin (a β-lactam) in inhibiting cell wall synthesis by preventing cross-linking of the forming peptidoglycans[91]. Obafluorin was identified as an antibacterial agent in 1984, but it was not until a recent analysis of the biosynthetic obafluorin operon that a possible mechanism of action was hypothesized for its antibacterial effects[49,50,52]. Within obafluorin's biosynthetic operon lies the gene *ObaO*, which encodes a TARS paralog of the same name (ObaO). One hypothesis for the function of this gene is that it may be an obafluorin resistant TARS paralog, as this would be necessary for *Pseudomonas fluorescens* to still produce $tRNA^{Thr}$ and thus have normal protein translation if obafluorin did inhibit TARS.

Borrelidin, an 18-membered macrolide compound with a five-membered ring attached to it at carbon 17, was isolated from *Streptomyces rocheii* in 1949[46]. Since then, its anti-malarial, anti-angiogenic, anti-fungal, and anti-tumor effects have been shown, the mechanism of these being its inhibition of TARS[43–47]. Like borrelidin, obafluorin may be a slow, tight binding inhibitor of TARS, but is yet to be kinetically characterized. To test the possible inhibitory effects of obafluorin on both bacterial and human TARS, we employed ARS kinetics assays and a wide range of obafluorin concentrations, allowing us to calculate the IC50 values for both enzymes.

4.2 Results

To validate obafluorin's hypothesized inhibitory effects on *E. coli* TARS' canonical function, four ARS kinetics assays were run, each with a different concentration of obafluorin (0 nm, 10 nm, 100 nm, and 1 µM). Increasing obafluorin concentration resulted in decreasing bacterial TARS activity, demonstrated by decreased progress curve slopes (Figure 15).

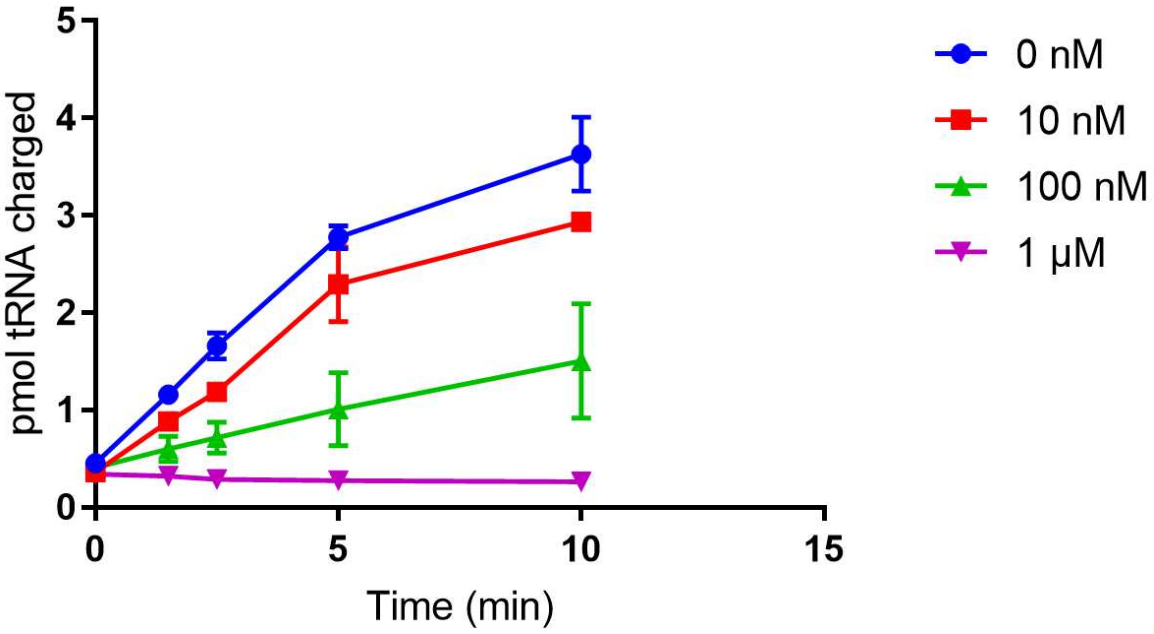

Figure 15. *E. coli* TARS is inhibited by obafluorin. N=3 Pmol of tRNA charged over time for four different ARS kinetics assays with *E. coli* TARS, each with a different concentration of obafluorin, shown in the figure key on the right. Error bars represent the standard error for each time point.

To better understand the inhibitory potential of obafluorin on bacterial TARS, more ARS kinetics assays were performed, but this time with seven different obafluorin concentrations and the end goal of creating an IC50 curve for obafluorin on bacterial TARS. Again, increasing obafluorin concentrations correlated with decreased bacterial TARS activity (Figure 16). From these data collected with 10 nM *E. coli* TARS, an IC50 value of $1.325*10^{-7}$ M (132.5 nM) was calculated (Figure 16) (Table 2).

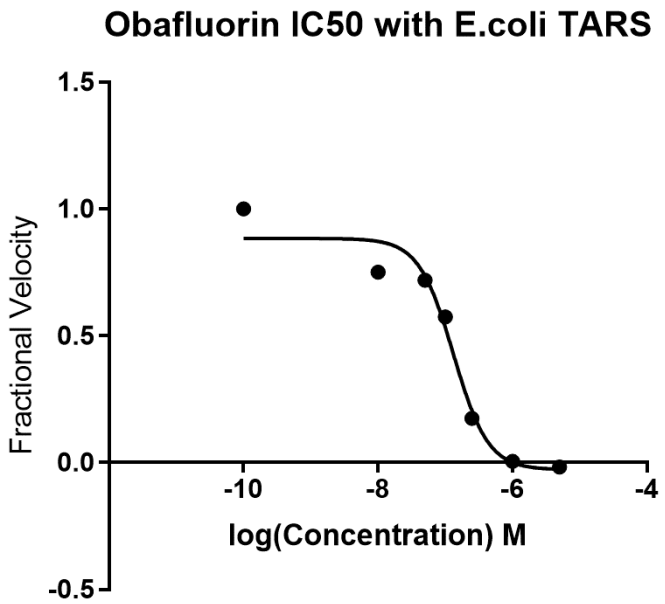

Figure 16. Obafluorin's IC50 with *E. coli* TARS. An IC50 curve for *E. coli* TARS with fractional velocity plotted against molar obafluorin concentration on a logarithmic scale. This curve was calculated from N=3 progress curve data with seven different obafluorin concentrations.

Table 2. Obafluorin IC50 values for *E. coli* and human TARS. Enzyme concentration, IC50 values and R^2 values from IC50 curves for both *E. coli* and human TARS. Experiments for IC50 curves were performed with N=3.

	***E. coli* TARS**	**Human TARS**
Enzyme concentration	10 nM	5 nM
IC50	$1.325*10^{-7}$ M (132.5 nM)	$2.396*10^{-8}$ M (23.96 nM)
R^2 value (non-linear fit, variable slope, four parameters)	0.9682	0.9683

Obafluorin's inhibitory potential on human TARS was then tested with seven ARS kinetics assays, each with a different obafluorin concentration (figure 17a). From this data collected with 5 nM human TARS, an IC50 value of $2.396*10^{-8}$ M (23.96 nM) was calculated (Figure 17b) (Table 2).

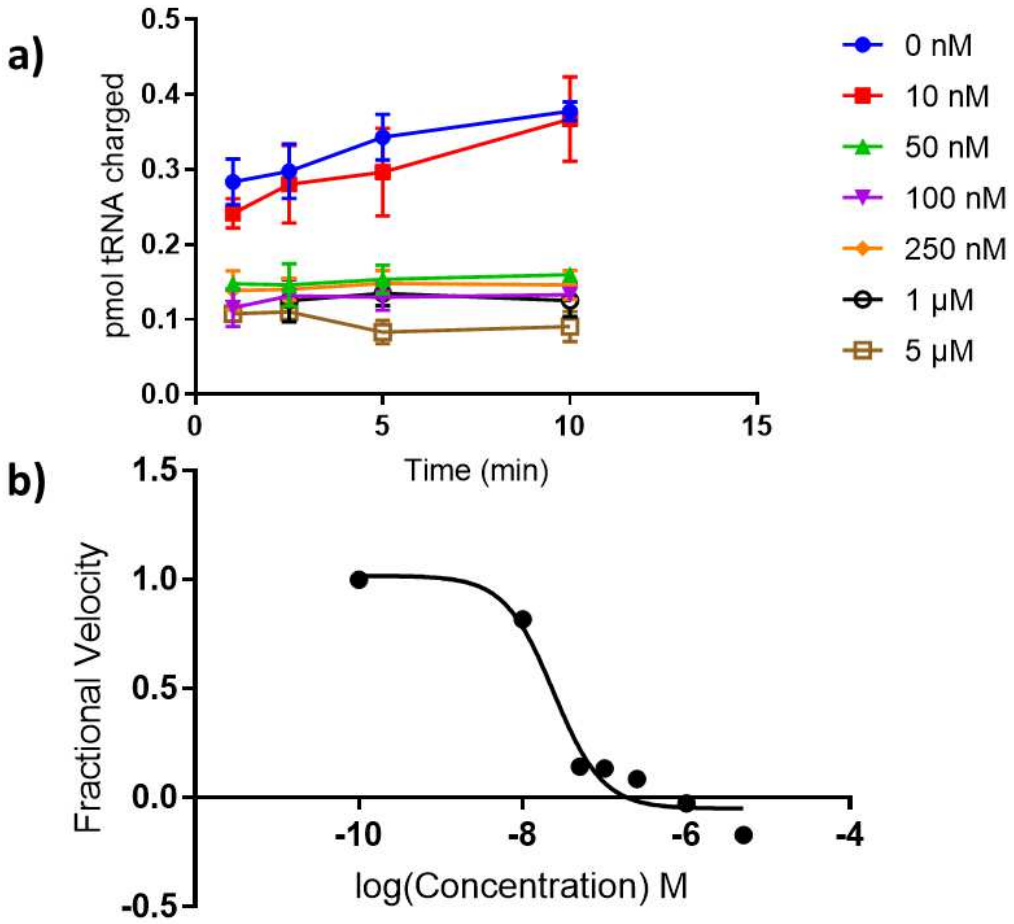

Figure 17. Obafluorin inhibits human TARS. a) Pmol of tRNA charged over time for seven different ARS kinetics assays with human TARS, each with a different concentration of obafluorin, shown in the figure legend on the right. Error bars represent the standard error for each time point. **N=3 b)** An IC50 curve for human TARS with fractional velocity plotted against molar obafluorin concentration on a logarithmic scale. This curve was calculated from N=3 progress curve data with seven different obafluorin concentrations.

Finally, the inhibitory potential of a benzoate obafluorin analog, EHTS-1, was tested for both bacterial and human TARS. ARS kinetics assays were performed with three different EHTS-1 concentrations for both bacterial and human TARS, yielding interesting results. EHTS-1 did not have a statistically significant inhibitory effect on human TARS (Figure 18a). The bacterial enzyme on the other hand did have significantly decreased activity in the presence of EHTS-1 (Figure 18b).

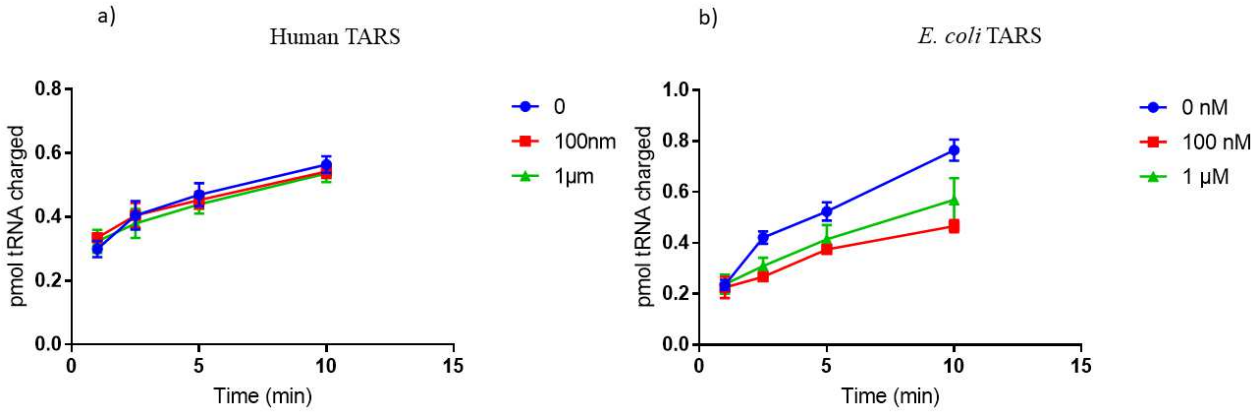

Figure 18. EHTS-1 inhibits *E. coli* TARS but not human TARS. a) Three ARS kinetics assay progress curves with *E. coli* TARS, each with a different obafluorin concentration. Error bars represent the standard error for each time point. Each curve was calculated from data of N=3. **b)** Three ARS kinetics assay progress curves with human TARS, each with a different obafluorin concentration. Error bars represent the standard error for each time point. Each curve was calculated from data of N=3.

Overall, many ARS kinetics assays across a range of obafluorin concentrations indicate that obafluorin does inhibit both *E. coli* and human TARS. Additionally, the benzoate obafluorin analog EHTS-1 did not have a statistically significant effect on human TARS, but did result in a significant decrease in *E. coli* TARS activity.

CHAPTER 5: DISCUSSION AND FUTURE DIRECTIONS

5.1: Autoaminoacylation

In this study, we validate and expand upon the finding of He et al., 2017, who described that ARS are capable of aminoacylating proteins. We find that *E. coli* TARS and HARS, as well as human TARS are capable of autoaminoacylation, and described the conditions required for this reaction to occur. The ATP dependence, activity increase in the presence of Mg^{2+}, specificity for each ARS's cognate amino acid and inhibition of TARS autoaminoacylation by increasing $tRNA^{Thr}$ concentrations suggest that this reaction occurs through the same mechanism as ARS's canonical tRNA charging function. This differs from the mechanism of protein aminoacylation discussed in Vo et al., 2018, where the protein ANKRD16 functions as a sink for Ser that has been mischarged by AlaRS[92]. When graphing aminoacylated *E. coli* TARS over time we observed a decrease in aminoacylated TARS after 3-4 hours of incubation (Figure 8b and 9b). This decrease in autoaminoacylation levels indicates that some of the isopeptide bonds formed in the aminoacylation reaction will break over time, and the plateau in aminoacylated TARS levels following it indicates that the reaction might reach an equilibrium between aminoacylated and un-aminoacylated ARS. In 1997 Gillet et al. demonstrated that aminoacylated MetRS displayed decreased aminoacylation functionality, supporting this hypothesis that the reaction reaches an equilibrium between unlabeled ARS and aminoacylated ARS that have decreased activity[57].

Though these findings are important in and of themselves, their implications about ARS as a means of post-translationally modifying proteins are far broader. If ARS are

capable of aminoacylating proteins, not only does this mean there is a new mechanism for PTM of proteins, there is also a new mechanism for PTM of proteins that is directly related to the amino acid pool of the cell[60]. This would allow aminoacylation to function as a signal for amino acid starvation or amino acid sufficiency conditions and play a role in the amino acid metabolism of the cell. Among the many aminoacylated proteins identified in Behrends et al. 2010, several pieces of the autophagy machinery are likely aminoacylated[72]. These include ATK101 from the ULK1 complex, PRKAG1 and 2 from AMPK γ, and ATG14, which is a part of the PI3K complex[72,93]. In a state of cellular amino acid sufficiency, ARS could label these proteins to propagate the amino acid sufficiency signal through the autophagy pathway, inhibiting it. In a state of cellular amino acid starvation, ARS would not be able to aminoacylate these pieces of autophagy machinery, allowing them to perform their typical function in the initiation of autophagy. Interestingly, ARS aminoacylation of proteins seems to be conserved between both prokaryotes (*E. coli)* and eukaryotes (humans). This points to this mechanism and PTM being very old, likely having a diverse range of functions across the tree of life[94].

One limitation to the methods employed in our study is the high background signal seen in our autoradiographs. Even after ensuring that our k-screens were blanked, and both the k-screens and cassettes were not radioactive, the background signal persisted in our autoradiographs. The background signal is likely a consequence of long k-screen exposure times (~60-80 hours) with a relatively weak radioisotope (^{14}C). With a stronger radioisotope we would see higher signal-to-noise ratio, which would allow QuantityOne to set a lower background radiation level while still showing where the signal was

concentrated on the screen. This does not diminish the impact of our findings, as there is a clear and quantifiable difference between conditions where autoaminoacylation was occurring and where it was not.

Alongside attempting to minimize background radiation in our autoradiographs, we would also like to test the effects of the TARS inhibitors BC194 and obafluorin on the autoaminoacylation reaction, as well as the effect of adding catalytically dead TARS mutants to the reaction mixture. By varying the concentration of catalytically dead TARS mutants in the reaction mixture, we could make a Michaelis-Menton curve for the reaction, as the catalytically dead mutants act exclusively as substrates for the reaction.

These autoaminoacylation experiments have been a piece of a much larger work that has the overarching goal of identifying the mechanisms underlying amino acid sensing in the autophagy pathway. Here, we have provided control experiments that confirm the results from Behrends et al., 2010 and He et al., 2017[60,72]. We would like to continue experiments like these by testing the ability of ARS to aminoacylate the components of the autophagy machinery put forth in Behrends et al., 2010, for example TARS aminoacylating a bacterially-expressed ULK1 catalytic domain construct[72]. Using immunoaffinity purification methods we could selectively purify ULK1 or other crucial components of autophagy machinery in both fed and starved conditions and compare whether the protein is aminoacylated via mass spectrometry to determine whether the modification is a function of the nutritional states of the cell. Alternatively, following immunoaffinity purification of components of autophagy machinery from amino acid starved conditions we could incubate the purified protein with select ARSs and either radiolabeled or ‘cold’ amino acid,

and detect the aminoacylation of these proteins by SDS page and autoradiography or mass spectrometry respectively.

Preliminary western blotting data indicates that leucine (Leu) or Thr depletion and TARS knockdown via siRNA significantly increase phosphorylated ULK1 (p-ULK1) at S555, indicating activation of autophagy. (Figure 19).

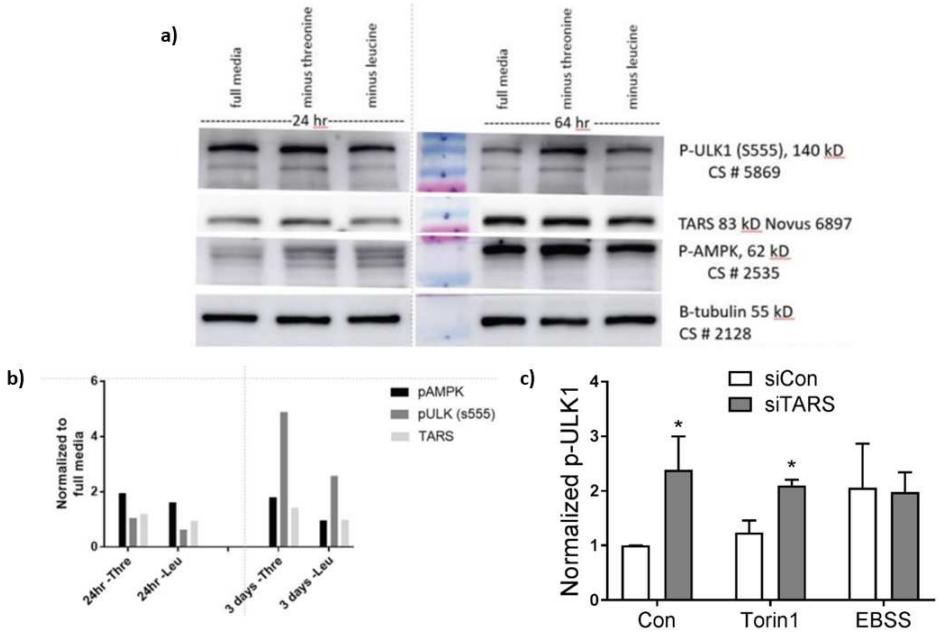

Figure 19. Amino acid depletion and TARS knockouts increase p-ULK1. a) Western blots against P-ULK1 (S555), TARS, P-AMPK, and β-tubulin in full media, and Thr and Leu deplete medias. **b)** Quantified western blot data showing phospho-AMPK (pAMPK), pULK1, and TARS levels in Thr and Leu starved media after 1 and 3 days. **c)** A bar graph showing normalized p-ULK1 levels from SKOV-3 cells in control media, Torin1 (an mTOR inhibitor) treated media, or amino acid starved media (EBSS) transfected with either control siRNA or siTARS.

Using human ovarian cancer cell lines (SKOV and PC12), siRNA against specific ARS, and amino acid rich and depleted medias, we will assess which ARSs and amino acids are most important in the process of autophagy initiation, detecting changes between fed and starved via well-validated autophagy assessment assays, including autophagy specific dyes[95], comparing free LC3 levels (a standard indicator of autophagy levels in the autophagy literature) vs LC3 levels in autophagosomes[96], or monitoring LC3 I maturation

to LC3 II[97]. We expect these experiments to support the essential branched chain amino acids being particularly crucial in the initiation of autophagy.

5.2: Obafluorin

In this study, we confirmed that obafluorin is an inhibitor of both *E. coli* and human TARS, and calculated IC50 values for obafluorin with both enzymes ($1.325*10^{-7}$ M (132.5 nM) at 10 nM enzyme concentration, and $2.396*10^{-8}$ M (23.96 nM) at 5 nM enzyme concentration respectively) (Table 2). We also showed that ETHS-1, a benzoate analog of obafluorin, did not have a statistically significant inhibitory effect on human TARS, but did result in a significant decrease in *E. coli* TARS activity.

TARS inhibitors often display antibacterial activities, including obafluorin [49]. This means that there is some potential for obafluorin and obafluorin analogs as antibacterial drugs, depending on their selectivity for the human and bacterial enzymes. Though calculated for different concentrations of enzyme (10 nM for *E. coli* and 5 nM for human), our preliminary data suggest that the human enzyme may have a higher affinity (lower IC50) for obafluorin than the bacterial enzyme. These data need more replicates and statistical support before publication, but if true, would indicate that obafluorin may not be useful as an antibacterial drug for use in humans, but may prove useful as an anti-angiogenic drug. TARS is among the several synthetases that have been implicated in angiogenesis, which when dysregulated is one of the hallmarks of cancer[34,37]. As a compound that has slightly more affinity to the human enzyme than the bacterial enzyme, obafluorin may prove useful as an anti-angiogenic drug with minimal off-target, gut-microbiota side effects. Alternatively, our data show that EHTS-1 had no significant

inhibitory effects on the human enzyme, but did significantly inhibit the bacterial enzyme (Figure 18). If supported with more replicates, enzyme concentrations and inhibitor concentrations, EHTS-1 could prove useful as an antibacterial drug for human use in the future.

This does bring up one drawback to our current data, the number of replicates necessary for statistical support of our data. Particularly highlighted in our EHTS-1 data with *E. coli* TARS (which shows that 100 nM EHTS-1 inhibited *E. coli* TARS significantly more than 1 μM EHTS-1 did), and in our obafluorin and human TARS IC50 curve (where the 5 μM obafluorin concentration had a negative fractional velocity), we need to repeat our experiments with more replicates, different enzyme preps, and more inhibitor concentrations to ensure accurate and reproducible IC50 values. Additionally, unpublished data from the Wilkinson lab has identified a gene encoding a TARS paralog within the cluster of genes involved with the obafluorin synthesis machinery. This enzyme, called ObaO, is largely similar to bacterial TARS, but has a Cys residue substituted for a Val. We hypothesize that this TARS paralog may be obafluorin resistant, and this Cys → Val substitution may be important for obafluorin resistance. We have been provided pET28a vectors that contain ObaO, ObaO with its Val substituted for a Cys, and *E. coli* TARS with its Cys substituted for a Val by the Wilkinson lab, and in future experiments we plan to test the effects of obafluorin on these three enzymes.

5.3: Closing Remarks

ARSs are a family of enzymes that are of critical importance for translation, attaching a specific amino acid to its cognate tRNA molecule. Recent ARS developments

range from elucidating their role in diseases from cancer to peripheral neuropathy, to exploring them as a means to post-translationally modify other proteins. This function is likely conserved across both prokaryotic and eukaryotic ARSs, opening up an incredibly diverse array of protein targets for ARSs to aminoacylate. Additionally, the discovery of new ARSs inhibitors that have different affinities for each ARSs ortholog offers unique possible solutions to the many diseases associated with ARSs. Here we have helped develop our understanding of ARSs as post-translational modifiers of pieces of the autophagy machinery and the novel TARS inhibitor obafluorin, expanding the already complex web of interactions and pathways that ARSs are involved in, and raising valuable questions that warrant the continued study of this diverse group of enzymes.

CHAPTER 6: BIBLIOGRAPHY

1. Szymanski, M., Deniziak, M. A. & Barciszewski, J. Aminoacyl-tRNA synthetases database. *Nucleic Acids Res.* **29,** 288–290 (2001).

2. Arnez, J. G. & Moras, D. Structural and functional considerations of the aminoacylation reaction. *Trends Biochem. Sci.* **22,** 211–216 (1997).

3. Berg, J. M., Tymoczko, J. L. & Stryer, L. Aminoacyl-Transfer RNA Synthetases Read the Genetic Code. (2002).

4. Eriani, G. *et al.* The class II aminoacyl-tRNA synthetases and their active site: evolutionary conservation of an ATP binding site. *J. Mol. Evol.* **40,** 499–508 (1995).

5. Ibba, M., Becker, H. D., Stathopoulos, C., Tumbula, D. L. & Söll, D. The adaptor hypothesis revisited. *Trends Biochem. Sci.* **25,** 311–316 (2000).

6. Carter, C. W. Coding of Class I and II Aminoacyl-tRNA Synthetases. *Adv. Exp. Med. Biol.* **966,** 103–148 (2017).

7. Martinez-Rodriguez, L. *et al.* Functional Class I and II Amino Acid-activating Enzymes Can Be Coded by Opposite Strands of the Same Gene. *J. Biol. Chem.* **290,** 19710–19725 (2015).

8. Li, R., Macnamara, L. M., Leuchter, J. D., Alexander, R. W. & Cho, S. S. MD Simulations of tRNA and Aminoacyl-tRNA Synthetases: Dynamics, Folding, Binding, and Allostery. *Int. J. Mol. Sci.* **16,** 15872–15902 (2015).

9. Abbott, J. A., Francklyn, C. S. & Robey-Bond, S. M. Transfer RNA and human disease. *Front. Genet.* **5,** 158 (2014).

10. Lee, J. W. *et al.* Editing-defective tRNA synthetase causes protein misfolding and neurodegeneration. *Nature* **443,** 50–55 (2006).

11. Karkhanis, V. A., Mascarenhas, A. P. & Martinis, S. A. Amino Acid Toxicities of Escherichia coli That Are Prevented by Leucyl-tRNA Synthetase Amino Acid Editing. *J. Bacteriol.* **189,** 8765–8768 (2007).

12. Jakubowski, H. & Goldman, E. Editing of errors in selection of amino acids for protein synthesis. *Microbiol. Rev.* **56,** 412–429 (1992).

13. Rajendran, V., Kalita, P., Shukla, H., Kumar, A. & Tripathi, T. Aminoacyl-tRNA synthetases: Structure, function, and drug discovery. *Int. J. Biol. Macromol.* **111,** 400–414 (2018).

14. Fersht, A. R. & Dingwall, C. Evidence for the double-sieve editing mechanism in protein synthesis. Steric exclusion of isoleucine by valyl-tRNA synthetases. *Biochemistry (Mosc.)* **18,** 2627–2631 (1979).

15. Sankaranarayanan, R. & Moras, D. The fidelity of the translation of the genetic code. *Acta Biochim. Pol.* **48,** 323–335 (2001).

16. Fersht, A. R. & Kaethner, M. M. Enzyme hyperspecificity. Rejection of threonine by the valyl-tRNA synthetase by misacylation and hydrolytic editing. *Biochemistry (Mosc.)* **15,** 3342–3346 (1976).

17. Minajigi, A. & Francklyn, C. S. Aminoacyl transfer rate dictates choice of editing pathway in threonyl-tRNA synthetase. *J. Biol. Chem.* **285,** 23810–23817 (2010).

18. Guo, M. & Schimmel, P. Essential Non-Translational Functions of tRNA Synthetases. *Nat. Chem. Biol.* **9,** 145–153 (2013).

19. Lo, W.-S. *et al.* Human tRNA synthetase catalytic nulls with diverse functions. *Science* **345,** 328–332 (2014).

20. Abbott, J. A. *et al.* The Usher Syndrome Type IIIB Histidyl-tRNA Synthetase Mutation Confers Temperature Sensitivity. *Biochemistry (Mosc.)* **56,** 3619–3631 (2017).

21. Kim, S., You, S. & Hwang, D. Aminoacyl-tRNA synthetases and tumorigenesis: more than housekeeping. *Nat. Rev. Cancer* **11,** 708–718 (2011).

22. White-Gilbertson, S., Kurtz, D. T. & Voelkel-Johnson, C. The role of protein synthesis in cell cycling and cancer. *Mol. Oncol.* **3,** 402–408 (2009).

23. Stephen, J. *et al.* Loss of function mutations in VARS encoding cytoplasmic valyl-tRNA synthetase cause microcephaly, seizures, and progressive cerebral atrophy. *Hum. Genet.* **137,** 293–303 (2018).

24. Charcot-Marie-Tooth Disease (CMT). *Muscular Dystrophy Association* (2015). Available at: https://www.mda.org/disease/charcot-marie-tooth. (Accessed: 30th April 2018)

25. Antonellis, A. *et al.* Glycyl tRNA synthetase mutations in Charcot-Marie-Tooth disease type 2D and distal spinal muscular atrophy type V. *Am. J. Hum. Genet.* **72,** 1293–1299 (2003).

26. Yao, P. & Fox, P. L. Aminoacyl-tRNA synthetases in medicine and disease. *EMBO Mol. Med.* **5,** 332–343 (2013).

27. Seburn, K. L., Nangle, L. A., Cox, G. A., Schimmel, P. & Burgess, R. W. An active dominant mutation of glycyl-tRNA synthetase causes neuropathy in a Charcot-Marie-Tooth 2D mouse model. *Neuron* **51,** 715–726 (2006).

28. Microcephaly Information Page | National Institute of Neurological Disorders and Stroke. Available at: https://www.ninds.nih.gov/Disorders/All-Disorders/Microcephaly-Information-Page. (Accessed: 30th April 2018)

29. Karaca, E. *et al.* Genes that Affect Brain Structure and Function Identified by Rare Variant Analyses of Mendelian Neurologic Disease. *Neuron* **88,** 499–513 (2015).

30. Siekierska, A. *et al.* Developmental encephalopathy with microcephaly linked to bi-allelic VARS variants is phenotypically recapitulated in a vars knockout zebrafish model.

31. Ibba, M., Francklyn, C. & Cusack, S. *The aminoacyl-tRNA synthetases*. (Landes Bioscience : Eurekah.com, 2005).

32. Marintchev, A. Fidelity and Quality Control in Gene Expression, Volume 86 - 1st Edition. (2012). Available at: https://www.elsevier.com/books/fidelity-and-quality-control-in-gene-expression/marintchev/978-0-12-386497-0. (Accessed: 21st April 2018)

33. Dock-Bregeon, A.-C. *et al.* Transfer RNA–Mediated Editing in Threonyl-tRNA Synthetase: The Class II Solution to the Double Discrimination Problem. *Cell* **103,** 877–884 (2000).

34. Mirando, A. C., Francklyn, C. S. & Lounsbury, K. M. Regulation of angiogenesis by aminoacyl-tRNA synthetases. *Int. J. Mol. Sci.* **15,** 23725–23748 (2014).

35. Adair, T. H. & Montani, J.-P. *Overview of Angiogenesis*. (Morgan & Claypool Life Sciences, 2010).

36. Williams, T. F., Mirando, A. C., Wilkinson, B., Francklyn, C. S. & Lounsbury, K. M. Secreted Threonyl-tRNA synthetase stimulates endothelial cell migration and angiogenesis. *Sci. Rep.* **3,** 1317 (2013).

37. Hanahan, D. & Weinberg, R. A. Hallmarks of Cancer: The Next Generation. *Cell* **144,** 646–674 (2011).

38. Garrett, R. & Grisham, C. *Biochemistry*. (Brooks/Cole, 2013).

39. Michaelis-Menten Kinetics. *Chemistry LibreTexts* (2013). Available at: https://chem.libretexts.org/Core/Biological_Chemistry/Catalysts/Enzymatic_Kinetics/Michaelis-Menten_Kinetics. (Accessed: 28th April 2018)

40. Ruan, B. *et al.* A Unique Hydrophobic Cluster Near the Active Site Contributes to Differences in Borrelidin Inhibition among Threonyl-tRNA Synthetases. *J. Biol. Chem.* **280,** 571–577 (2005).

41. Copeland, R. *Evaluation of Enzyme Inhibitors in Drug Discovery, A Guide for Medicinal Chemists and Pharmacologists*. (Wiley, 2013).

42. Mirando, A. C. *et al.* Aminoacyl-tRNA synthetase dependent angiogenesis revealed by a bioengineered macrolide inhibitor. *Sci. Rep.* **5,** 13160 (2015).

43. Tsuchiya, E., Yukawa, M., Miyakawa, T., Kimura, K. I. & Takahashi, H. Borrelidin inhibits a cyclin-dependent kinase (CDK), Cdc28/Cln2, of Saccharomyces cerevisiae. *J. Antibiot. (Tokyo)* **54,** 84–90 (2001).

44. Otoguro, K. *et al.* In vitro and in vivo antimalarial activities of a non-glycosidic 18-membered macrolide antibiotic, borrelidin, against drug-resistant strains of Plasmodia. *J. Antibiot. (Tokyo)* **56,** 727–729 (2003).

45. Funahashi, Y. *et al.* Establishment of a quantitative mouse dorsal air sac model and its application to evaluate a new angiogenesis inhibitor. *Oncol. Res.* **11,** 319–329 (1999).

46. Berger, J., Jampolsky, L. M. & Goldberg, M. W. Borrelidin, a new antibiotic with antiborrelia activity and penicillin enhancement properties. *Arch. Biochem.* **22,** 476–478 (1949).

47. Anderton, K. & Rickards, R. W. Some structural features of borrelidin, an anti-viral antibiotic. *Nature* **206,** 269 (1965).

48. Paetz, W. & Nass, G. Biochemical and immunological characterization of threonyl-tRNA synthetase of two borrelidin-resistant mutants of Escherichia coli K12. *Eur. J. Biochem.* **35,** 331–337 (1973).

49. Wells, J. S., Trejo, W. H., Principe, P. A. & Sykes, R. B. Obafluorin, a novel beta-lactone produced by Pseudomonas fluorescens. Taxonomy, fermentation and biological properties. *J. Antibiot. (Tokyo)* **37,** 802–803 (1984).

50. Tymiak, A. A., Culver, C. A., Malley, M. F. & Gougoutas, J. Z. Structure of obafluorin: an antibacterial beta-lactone from Pseudomonas fluorescens. *J. Org. Chem.* **50,** 5491–5495 (1985).

51. Pubchem. Obafluorin. Available at: https://pubchem.ncbi.nlm.nih.gov/compound/146354. (Accessed: 18th April 2018)

52. Scott, T. A., Heine, D., Qin, Z. & Wilkinson, B. An L-threonine transaldolase is required for L-threo-β-hydroxy-α-amino acid assembly during obafluorin biosynthesis. *Nat. Commun.* **8,** 15935 (2017).

53. Christopher T. Walsh. *Posttranslational Modification of Proteins. Expanding Nature's Inventory.* (Roberts and Company, 2006).

54. Dell, A., Galadari, A., Sastre, F. & Hitchen, P. Similarities and Differences in the Glycosylation Mechanisms in Prokaryotes and Eukaryotes. *International Journal of Microbiology* (2010). doi:10.1155/2010/148178

55. Kim, B. S., Lee, C.-H., Chang, G.-E., Cheong, E. & Shin, I. A potent and selective small molecule inhibitor of sirtuin 1 promotes differentiation of pluripotent P19 cells into functional neurons. *Sci. Rep.* **6,** 34324 (2016).

56. Gautam, R., Akam, E. A., Astashkin, A. V., Loughrey, J. J. & Tomat, E. Sirtuin inhibitor sirtinol is an intracellular iron chelator. *Chem. Commun. Camb. Engl.* **51,** 5104–5107 (2015).

57. Gillet, S., Hountondji, C., Schmitter, J.-M. & Blanquet, S. Covalent methionylation of escherichia coli methionyl-tRNA synthethase: Identification of the labeled amino acid residues by matrix-assisted laser desorption-ionization mass spectrometry. *Protein Sci.* **6,** 2426–2435 (1997).

58. Hountondji, C., Beauvallet, C., Pernollet, J. C. & Blanquet, S. Enzyme-induced covalent modification of methionyl-tRNA synthetase from Bacillus stearothermophilus by methionyl-adenylate: identification of the labeled amino acid residues by matrix-assisted laser desorption-ionization mass spectrometry. *J. Protein Chem.* **19,** 563–568 (2000).

59. Yanagisawa, T., Sumida, T., Ishii, R., Takemoto, C. & Yokoyama, S. A paralog of lysyl-tRNA synthetase aminoacylates a conserved lysine residue in translation elongation factor P. *Nat. Struct. Mol. Biol.* **17,** 1136–1143 (2010).

60. He, X.-D. *et al.* Sensing and Transmitting Intracellular Amino Acid Signals through Reversible Lysine Aminoacylations. *Cell Metab.* **0,** (2017).

61. Colak, G. *et al.* Identification of lysine succinylation substrates and the succinylation regulatory enzyme CobB in Escherichia coli. *Mol. Cell. Proteomics MCP* **12,** 3509–3520 (2013).

62. Hurley, J. H. & Young, L. N. Mechanisms of Autophagy Initiation. *Annu. Rev. Biochem.* **86,** 225–244 (2017).

63. Glick, D., Barth, S. & Macleod, K. F. Autophagy: cellular and molecular mechanisms. *J. Pathol.* **221,** 3–12 (2010).

64. Kaushik, S. & Cuervo, A. M. Chaperone-mediated autophagy: a unique way to enter the lysosome world. *Trends Cell Biol.* **22,** 407–417 (2012).

65. Li, W., Li, J. & Bao, J. Microautophagy: lesser-known self-eating. *Cell. Mol. Life Sci. CMLS* **69,** 1125–1136 (2012).

66. Kim, K. H. & Lee, M.-S. Autophagy--a key player in cellular and body metabolism. *Nat. Rev. Endocrinol.* **10,** 322–337 (2014).

67. Antonioli, M., Di Rienzo, M., Piacentini, M. & Fimia, G. M. Emerging Mechanisms in Initiating and Terminating Autophagy. *Trends Biochem. Sci.* **42,** 28–41 (2017).

68. Zaffagnini, G. & Martens, S. Mechanisms of Selective Autophagy. *J. Mol. Biol.* **428,** 1714–1724 (2016).

69. Khaminets, A., Behl, C. & Dikic, I. Ubiquitin-Dependent And Independent Signals In Selective Autophagy. *Trends Cell Biol.* **26,** 6–16 (2016).

70. Bar-Peled, L. & Sabatini, D. M. Regulation of mTORC1 by amino acids. *Trends Cell Biol.* **24,** 400–406 (2014).

71. Hara, K. *et al.* Amino acid sufficiency and mTOR regulate p70 S6 kinase and eIF-4E BP1 through a common effector mechanism. *J. Biol. Chem.* **273,** 14484–14494 (1998).

72. Behrends, C., Sowa, M. E., Gygi, S. P. & Harper, J. W. Network organization of the human autophagy system. *Nature* **466,** 68–76 (2010).

73. Choi, A. M. K., Ryter, S. W. & Levine, B. Autophagy in Human Health and Disease. *N. Engl. J. Med.* **368,** 651–662 (2013).

74. Parkes, M. *et al.* Sequence variants in the autophagy gene IRGM and multiple other replicating loci contribute to Crohn's disease susceptibility. *Nat. Genet.* **39,** 830–832 (2007).

75. Chauhan, S., Mandell, M. A. & Deretic, V. IRGM governs the core autophagy machinery to conduct antimicrobial defense. *Mol. Cell* **58,** 507–521 (2015).

76. Hampe, J. *et al.* A genome-wide association scan of nonsynonymous SNPs identifies a susceptibility variant for Crohn disease in ATG16L1. *Nat. Genet.* **39,** 207–211 (2007).

77. Salem, M., Ammitzboell, M., Nys, K., Seidelin, J. B. & Nielsen, O. H. ATG16L1: A multifunctional susceptibility factor in Crohn disease. *Autophagy* **11,** 585–594 (2015).

78. ATG16L1 - Autophagy-related protein 16-1 - Homo sapiens (Human) - ATG16L1 gene & protein. Available at: https://www.uniprot.org/uniprot/Q676U5. (Accessed: 18th May 2018)

79. Chen, D. *et al.* Genetic analysis of the ATG7 gene promoter in sporadic Parkinson's disease. *Neurosci. Lett.* **534,** 193–198 (2013).

80. Chen, D. *et al.* A novel and functional variant within the ATG5 gene promoter in sporadic Parkinson's disease. *Neurosci. Lett.* **538,** 49–53 (2013).

81. Lee, J.-H. *et al.* Lysosomal proteolysis and autophagy require presenilin 1 and are disrupted by Alzheimer-related PS1 mutations. *Cell* **141,** 1146–1158 (2010).

82. Galluzzi, L. *et al.* Autophagy in malignant transformation and cancer progression. *EMBO J.* **34,** 856–880 (2015).

83. Avivar-Valderas, A. *et al.* Regulation of autophagy during ECM detachment is linked to a selective inhibition of mTORC1 by PERK. *Oncogene* **32,** 4932–4940 (2013).

84. Qu, X. *et al.* Promotion of tumorigenesis by heterozygous disruption of the beclin 1 autophagy gene. *J. Clin. Invest.* **112,** 1809–1820 (2003).

85. Yue, Z., Jin, S., Yang, C., Levine, A. J. & Heintz, N. Beclin 1, an autophagy gene essential for early embryonic development, is a haploinsufficient tumor suppressor. *Proc. Natl. Acad. Sci. U. S. A.* **100,** 15077–15082 (2003).

86. Pasman, Z. *et al.* Substrate specificity and catalysis by the editing active site of Alanyl-tRNA synthetase from Escherichia coli. *Biochemistry (Mosc.)* **50,** 1474–1482 (2011).

87. Yan, W., Augustine, J. & Francklyn, C. A tRNA identity switch mediated by the binding interaction between a tRNA anticodon and the accessory domain of a class II aminoacyl-tRNA synthetase. *Biochemistry (Mosc.)* **35,** 6559–6568 (1996).

88. Minajigi, A. & Francklyn, C. S. RNA-assisted catalysis in a protein enzyme: The 2'-hydroxyl of tRNA(Thr) A76 promotes aminoacylation by threonyl-tRNA synthetase. *Proc. Natl. Acad. Sci. U. S. A.* **105,** 17748–17753 (2008).

89. Milligan, J. F., Groebe, D. R., Witherell, G. W. & Uhlenbeck, O. C. Oligoribonucleotide synthesis using T7 RNA polymerase and synthetic DNA templates. *Nucleic Acids Res.* **15,** 8783–8798 (1987).

90. Francklyn, C. S., First, E. A., Perona, J. J. & Hou, Y.-M. Methods for kinetic and thermodynamic analysis of aminoacyl-tRNA synthetases. *Methods San Diego Calif* **44,** 100–118 (2008).

91. Kong, K.-F., Schneper, L. & Mathee, K. Beta-lactam Antibiotics: From Antibiosis to Resistance and Bacteriology. *APMIS Acta Pathol. Microbiol. Immunol. Scand.* **118,** 1–36 (2010).

92. Vo, M.-N. *et al.* ANKRD16 prevents neuron loss caused by an editing-defective tRNA synthetase. *Nature* **557,** 510–515 (2018).

93. Diao, J. *et al.* ATG14 promotes membrane tethering and fusion of autophagosomes to endolysosomes. *Nature* **520,** 563–566 (2015).

94. Beltrao, P., Bork, P., Krogan, N. J. & Noort, V. van. Evolution and functional cross□talk of protein post□translational modifications. *Mol. Syst. Biol.* **9,** 714 (2013).

95. Chan, L. L.-Y. *et al.* A novel image-based cytometry method for autophagy detection in living cells. *Autophagy* **8,** 1371–1382 (2012).

96. Kimura, S., Fujita, N., Noda, T. & Yoshimori, T. Monitoring autophagy in mammalian cultured cells through the dynamics of LC3. *Methods Enzymol.* **452,** 1–12 (2009).

97. Rodríguez-Arribas, M., Yakhine-Diop, S. M. S., González-Polo, R. A., Niso-Santano, M. & Fuentes, J. M. Turnover of Lipidated LC3 and Autophagic Cargoes in Mammalian Cells. *Methods Enzymol.* **587,** 55–70 (2017).

98. Latour, P. *et al.* A Major Determinant for Binding and Aminoacylation of tRNAAla in Cytoplasmic Alanyl-tRNA Synthetase Is Mutated in Dominant Axonal Charcot-Marie-Tooth Disease. *Am. J. Hum. Genet.* **86,** 77–82 (2010).

99. Safka Brozkova, D. *et al.* Loss of function mutations in HARS cause a spectrum of inherited peripheral neuropathies. *Brain J. Neurol.* **138,** 2161–2172 (2015).

100. Vester, A. *et al.* A loss-of-function variant in the human histidyl-tRNA synthetase (HARS) gene is neurotoxic in vivo. *Hum. Mutat.* **34,** 191–199 (2013).

101. McMillan, H. J. *et al.* Congenital Visual Impairment and Progressive Microcephaly Due to Lysyl-Transfer Ribonucleic Acid (RNA) Synthetase (KARS) Mutations: The Expanding Phenotype of Aminoacyl-Transfer RNA Synthetase Mutations in Human Disease. *J. Child Neurol.* **30,** 1037–1043 (2015).

102. Zhang, X. *et al.* Mutations in QARS, encoding glutaminyl-tRNA synthetase, cause progressive microcephaly, cerebral-cerebellar atrophy, and intractable seizures. *Am. J. Hum. Genet.* **94,** 547–558 (2014).

103. Salvarinova, R. *et al.* Expansion of the QARS deficiency phenotype with report of a family with isolated supratentorial brain abnormalities. *Neurogenetics* **16,** 145–149 (2015).

APPENDIX: CHARACTERIZING THE ACTIVITY OF VALYL-TRNA SYNTHETASE MUTANTS

Intro:

As a result of ARSs integral role in protein translation and their growing list of secondary functions, many ARS have been implicated in many different diseases, ranging from cancer and autoimmune diseases to neurodegenerative diseases[9,21]. Both dominant and recessive pathogenic variants have been identified in ARS genes from patients with disorders presenting neurological features. These range from diseases with peripheral neuropathies like Charcot Marie Tooth Syndrome[98–100], to congenital visual impairment with progressive microcephaly[101], and developmental delays with progressive microcephaly and intractable seizures[102,103]. Recently, several novel VARS variants were identified in mainly consanguineous families, two families of which were previously reported as VARS being a candidate 'disease gene'[29]. Several of these mutant variants were tested via yeast complementation assays and in zebrafish models, demonstrating that these variants likely lead to a loss of protein function and that VARS deficiency mirrors some of the main characteristics of the human disease. To supplement the yeast complementation data and further support the recently identified VARS variants cause a loss of function, we performed *in vitro* activity assays on patient-derived fibroblasts and lymphoblasts. Our assays supported the hypothesis that these new VARS variants have a loss of function and that they may be contributing to the phenotypes displayed by the patents. If it was the case that the parents did not have 100% activity compared to control, this would suggest that there is a threshold below which loss of aminoacylation activity causes disease phenotype,

and mutations that allow aminoacylation function above this threshold will be non-pathogenic. Determining this threshold could be useful for predicting the possible phenotypes that could manifest in a patient containing specific mutations.

Methods:

These protocols were modified from the aminoacylation protocol described in Puffenberger et al. 2012. Control ATCC cells and patient derived cell samples were grown in Dulbecco's Modified Eagle Medium, high glucose (Gibco®) enriched with 10% heat-inactivated Fetal Bovine serum (FBS) (Gibco®), 1% L-glutamine (Life Technologies), 1% penicillin-streptomycin (Life Technologies) conditions for fibroblasts and RPMI 1640 Medium (Gibco®), enriched with 10% heat-inactivated FBS (Gibco®), 1% L-glutamine (Life Technologies), 1% penicillin-streptomycin (Life Technologies) and 1% sodium pyruvate (Life Technologies) conditions for lymphoblasts. Following washes with Dulbecco's phosphate buffered saline, cells were lysed in protease inhibitor cocktail (Sigma), 50 mM Tris-HCl pH 7.5, 150 mM NaCl, 5 mM dithioreitol, and 0.5% Triton X-100 and protein concentration was measured via Bradford assay. Lysates were mixed to make 100 mM HEPES pH 7.2, 30 mM KCl, 10 mM $MgCl_2$, 107 μM total human placental tRNA, 2 mM ATP, 50 μM ^{14}C-labeled valine (282.8 mCi/mmol). These mixes were incubated at 37 ^{o}C with timepoints taken at 1, 2.5, 5 and 10 minutes of incubation. These timepoints were quenched when spotted onto 3MM Whatman filter paper pre-soaked with 5% TCA. This filter paper was washed three times with 5% TCA, and once with 95% ethanol before having its radiation quantified via liquid scintillation. The specific activity

for each sample was calculated from linear fits of progress curve data, and was subsequently corrected for total protein concentration.

Results and Discussion:

Using the above assay on the available patient lymphoblasts and fibroblasts, all the patient cells tested showed decreased VARS activity (Figure 20).

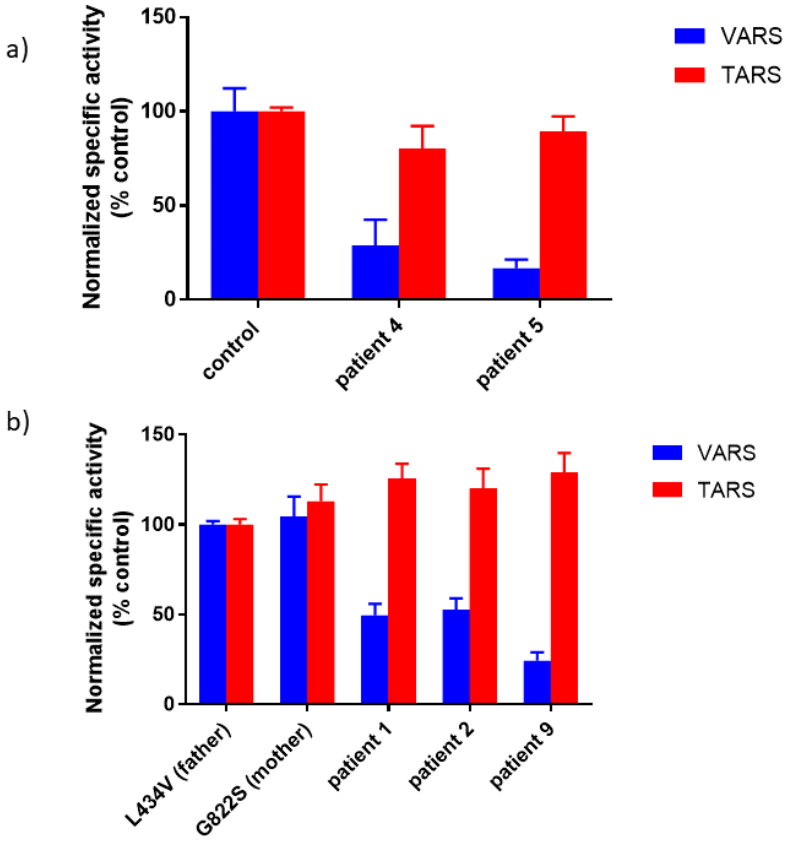

Figure 20. Patient cells have decreased VARS activity. VARS and TARS activity levels measured from control or patient cell cell lysates. Error bars represent the standard error for each data set. Fibroblast data is in a), lymphoblast data is in b).

In the fibroblasts, patients 4 and 5 (heterozygous carrying the p.Leu78Argfs*35/p.Arg942Gln variants) each display significantly decreased activity compared to control cells, approximately 25% and 12.5% respectively (Figure 20a).

Looking at the lymphoblasts, Patients 1 and 2 (heterozygous carrying the p.Leu434Val/p.Gly828Ser variants) had approximately 50% VARS activity compared to their parents (who did not display the phenotype but were heterozygous carrying the wild-type allele and either the p.Leu434Val or p.Gly828Ser variant) (Figure 20b). Patient 9 (carrying homozygous p.Arg404Trp variant) had approximately 25% VARS activity compared to the mother and father. The heterozygosity of each parent (having one wild-type allele and either p.Leu434Val or p.Gly828Ser each) raises the question as to whether the parents have the same activity levels as a control cell line that is homozygous for wild-type VARS. If it was the case that the parents did not have 100% activity compared to control, this would suggest that there is a threshold of aminoacylation activity for displaying a phenotype, which could in turn be useful for predicting the possible phenotypes that could manifest in a patient containing specific mutations.

These results support the variants expressed in the tested patient cells being loss of function variants, and along with zebrafish and yeast complementation data collected for these variants, suggest that these variants may be the mechanism underlying neurological disease phenotypes displayed by these families[30]. This was among the first kinetic assays of VARS in association neurological disease, and provides us some basis for possible prediction of phenotypes that may be associated with ARS variants, better understanding the phenotypes of the afflicted patients, and perhaps future therapies for the observed phenotypes.